

Adaptive, Anthropomorphic Robot Hands for Grasping and In-Hand Manipulation

Georgios P. Kontoudis

Thesis submitted to the Faculty of the
Virginia Polytechnic Institute and State University
in partial fulfillment of the requirements for the degree of

Master of Science

in

Mechanical Engineering

Tomonari Furukawa, Chair

Alexander Leonessa

Alan T. Asbeck

Kyriakos G. Vamvoudakis

December 10, 2018

Blacksburg, Virginia

Keywords: Underactuation, Tendon-Driven Mechanisms, Monolithic Fingers,
Anthropomorphic Robot Hands, Grasping, In-Hand Manipulation.

Adaptive, Anthropomorphic Robot Hands for Grasping and In-Hand Manipulation

Georgios P. Kontoudis

Academic Abstract

This thesis presents the design, modeling, and development of adaptive robot hands that are capable of performing dexterous, in-hand manipulation. The robot hand comprises of anthropomorphic robotic fingers, which employ an adaptive actuation mechanism. The mechanism achieves both flexion/extension and adduction/abduction, on the finger's metacarpophalangeal joint, by using two actuators. Moment arm pulleys are employed to drive the tendon laterally, such that an amplification on the abduction motion occurs, while also maintaining the flexion motion. Particular emphasis has been given to the modeling and the analysis of the actuation mechanism. Also, a model for spatial motion is provided that relates the actuation modes with the finger motion and the tendon force with the finger characteristics. For the hand design, the use of differential mechanisms simplifies the actuation scheme, as we utilize only two actuators for four fingers, achieving affordable dexterity. A design optimization framework assess the results of hand anthropometry studies to derive key parameters for the bio-inspired actuation design. The model assumptions are evaluated with the finite element method. The proposed finger has been fabricated with the Hybrid Deposition Manufacturing technique and the actuation mechanism's efficiency has been validated with experiments that include the computation of the finger workspace, the assessment of the force exertion capabilities, the demonstration of the feasible motions, and the grasping and manipulation capabilities. Also, the hand design is fabricated with off-the-shelf materials and rapid prototyping techniques while its efficiency has been validated using an extensive set of experimental paradigms that involved the execution of grasping and in-hand manipulation tasks with everyday objects.

Adaptive, Anthropomorphic Robot Hands for Grasping and In-Hand Manipulation

Georgios P. Kontoudis

General Audience Abstract

This thesis presents the design, modeling, and development of adaptive robot hands that are capable of performing selective interdigitation, robust grasping, and dexterous, in-hand manipulation. The robotic fingers employ an adaptive actuation mechanism. The design is minimal and the hand is capable of performing selective interdigitation, robust grasping, and dexterous, in-hand manipulation. Particular emphasis has been given to the modeling and the analysis of the actuation mechanism. For the hand design, the use of differential mechanisms simplifies the actuation scheme, as we utilize only two actuators for four fingers, achieving affordable dexterity. A design optimization framework assess the results of hand anthropometry studies to derive key parameters for the actuation design. The robotic fingers and the anthropomorphic hand were fabricated using off-the-shelf materials and additive manufacturing techniques. Several experiments were performed to validate the efficacy of the robot hand.

Dedication

To my parents and my sister.

Acknowledgments

I would like to thank my advisor Prof. Tomonari Furukawa for his continuous guidance during the past two years. Moreover, I would like to thank Prof. Vamvoudakis for giving me the opportunity to work with him, his friendship, and for his crucial advices. Thanks to my committee, Prof. Leonessa, and Prof. Asbeck for their support.

I would like to thank Prof. Minas Liarokapis for his crucial guidance and mentorship throughout my career. He is a real friend and his support is endless.

Thanks to my labmates in the Computational Multiphysics Systems Lab, Cameron Ridgewell, Peter Amico, Tamer Atia, Josiah Steckenrider, Jonathan Hodges, Cong Chen, Rich Fedora, Chris Mobley, Ioannis Papakis, Mengyu Song, Jeeseop Kim, Ashrarul Sifat, Mickey Cowden, Urvi Desai, Diya Li, Murat Ambarkutuk, Yazhe Hu, Karim Abdelatty, Jihong Cai, Haseeb Chaudhry, Boren Li, and Orson Lin who contributed in my education and helped me to improve my research.

I would like to thank my best friends, Vaggelis Kokorakis, Thodoris Theotokis, Lorentzos Mikroutikos, and Serafeim Chasomeris for being the best company and for giving me great advices about my life.

My girlfriend for her love, moral support, and tolerance on the long hours I spent in the lab and short hours with her. She is my other half and left Greece to join me at Virginia Tech. I hope to make up for our sacrifices soon.

Finally, I would like to thank my family, Ksanthi Kontoudi, Pantelis Kontoudis, Mairy Kontoudi, Stelios Katsourinis, Sotiris Katsourinis, and Ksanthi Katsourini for their endless love, and their continuous support at every step of my life.

Contents

List of Figures	ix
List of Tables	xiv
1 Introduction	1
1.1 Grasping and In-Hand Manipulation	1
1.2 Objectives	1
1.3 Contributions	2
1.4 List of Publications	3
1.5 Outline	4
2 Literature Review	5
2.1 Robotic Fingers	5
2.2 Anthropomorphic Robot Hands	6
2.3 Summary	9
3 Finger Design	10
3.1 Actuation Mechanism Design	10
3.2 Rigid Body Modeling	13

3.3	Actuation Mechanism Modeling and Analysis	16
3.4	Developed Finger	23
3.5	Summary	25
4	Robot Hand Design	26
4.1	Differential Mechanism Design	26
4.2	Design Optimization	27
4.3	Fabrication Process	31
4.4	Summary	35
5	Results and Experiments	36
5.1	Finger Experiments	37
5.1.1	Finite Element Method	37
5.1.2	Finger Postures	38
5.1.3	Force Exertion Capabilities	39
5.1.4	Finger Workspace	40
5.1.5	Finger Grasping and Manipulation Capabilities	42
5.2	Hand Experiments	43
5.2.1	Hand Postures and Gestures	43
5.2.2	Grasping Everyday Life Objects	44
5.2.3	Dexterous Manipulation	45

5.3 Summary	45
6 Conclusions and Future Work	47
Bibliography	49

List of Figures

3.1	An exploded view of the finger’s 3D model design. The finger is compliant as it employs elastomer material to implement the flexure joints. The design modularity is reflected by using a single bolt-nut set to connect to the palm.	11
3.2	The actuation mechanism that allows for F/E and A/A concurrently. This finger operates with clockwise motion. For counterclockwise motion, the right side anchor point needs to be swiftd on the left side. For bidirectional abduction, the central anchor point needs to be placed on the left side of the finger.	12
3.3	The mechanical model of a compliant finger that achieves a clockwise rotation. The flexure joints were modeled as a spring-damper and each phalange as a mass. The flexion/extension of the DIP, PIP, and MCP joints reflects the x_d , x_p , and x_{fm} motions respectively, while the adduction/abduction occurs towards the θ rotational direction.	13
3.4	A model of the robotic finger for computing the gravity compensation with a torsion spring.	14

3.5	The actuation mechanism in various configurations. Different design choices with respect to the moment arm pulley position, produce various abduction motions. (a) The moment arm pulley is perpendicular with the tendon guide pin. (b) The moment arm pulley is in an intermediate position. (c) The distance from the joint axis of rotation to the moment arm pulley r_{am} matches the radius length r . (d) The distance from the joint axis of rotation to the moment arm pulley r_{am} is higher than the radius length r	17
3.6	The actuation mechanism model at the initial and at the maximum abduction configuration. (a) The mechanism characteristics at the initial configuration. (b) The mechanism characteristics at the maximum abduction angle. (c) The mechanism characteristics at the maximum abduction angle. (d) The mechanism characteristics focused on the tendon guide pin at the maximum abduction angle.	19
3.7	The finger model for spatial motion. (a) The abduction θ_{MCP} is performed from the abduction actuator f_{aa} . (b) The flexion is occurred either from the flexion actuator f_{fa} , or from the combined motion of both actuators, or from the abduction actuator when $\theta_{MCP} > \theta_{max}$	22
3.8	The fabrication porcess of the developed finger. (a) The reusable mold in blue, the rotating base in purple, and the sacrificial mold in black. (b) The elastomer material at the curing phase. (c) Side views and front view of the fabricated finger.	24

4.1	The two parallel differential mechanisms based on the Whiffletree. The differential mechanism comprises of three bars. One bar to actuate the index and middle fingers, one bar to actuate the ring and pinky fingers, and the main bar to connect the actuator with the two bars. The first tendon-routing system is responsible for the F/E of the four fingers and the second tendon-routing system performs A/A on three fingers.	27
4.2	The design optimization parameters of the proposed differential mechanism. The two top bars are responsible for the index and the ring-pinky A/A motions. The blocked finger is depicted as solid black circle. The main bar connects the 2 top bars with the actuator. The attachment points are located in the center of all bars.	28
4.3	The alteration of differential motion according to the design characteristics. The length reduction on the blocked index bar generates larger differential motion (δy_i) for the same actuator displacement (d_{ai}). (a) The 2 top bars have the same length. (b) The bar that is related with index digit's motion is shorter than the other top (ring-pinky) bar.	31
4.4	The representation of the Kapandji test (a) Thumb fingertip in contact with the pinky MCP base frame. (b) Thumb fingertip in contact with the index MCP base frame. (c) Thumb fingertip in contact with the pinky fingertip and without any flexion on the PIP and DIP joints. (d) Thumb fingertip in contact with the index fingertip and without any flexion on the PIP and DIP joints.	34

5.1	Flexion response of the monolithic adaptive finger with FEM. (a) Finger flexed in the free space. (b) Finger flexed while in contact with an obstacle that constraints the MCP flexure joint motion.	37
5.2	The anthropomorphic finger in various configurations. (a) Finger in the neutral (rest) position. (b) Finger abduction by using the corresponding tendon-driven system. (c) Finger flexion without any abduction. (d) Finger flexion in an abducted angle.	38
5.3	The experimental setup for measuring the finger force capabilities.	39
5.4	The comparison of the forces exerted by the fingertip in two different configurations. The finger reports competitive exerted forces even at fully abducted position. The decay after the overshoot represents the strain energy stored in the elastomer material of the flexure joints.	40
5.5	The reachable workspace of an anthropomorphic index finger. The triangles represent the position of the joints through time. (a) Perspective view. (b) The top view illustrates the finger abduction. (c) The side view depicts the finger flexion.	41
5.6	The anthropomorphic finger performing a manipulation task. (a) The adaptive finger with the cylindrical object. (b) Initial grasping position. (c) Rolling clockwise 45°. (d) Rolling counterclockwise 90°.	42
5.7	Grasping postures and gestures executed by the proposed adaptive robot hand. The A/A capabilities are depicted in the first row. The second row of images shows the implementation of the Kapandji test.	43

5.8	The proposed adaptive robot hand while performing grasping experiments with various everyday life objects. More precisely, the grasps involve a) an egg, b) a large rectangular object, c) a plastic cylindrical object, d) a ruler, e) a pair of sunglasses, f) a small plastic ball, g) a banana, and h) a bottle of water.	44
5.9	An equilibrium point manipulation experiment executed with the proposed robot hand. The robot hand successfully grasps a spherical object and then performs rolling of the object. Yet, the rolling is not simple and results also to equilibrium point motion, which is one of the most challenging dexterous manipulation tasks.	45

List of Tables

4.1	Finger Dimensions of Robot Hand	32
4.2	Finger Joint Radii	33
4.3	Finger Joint Rotational Stiffness	34
4.4	Robot Hand Characteristics	35

Chapter 1

Introduction

1.1 Grasping and In-Hand Manipulation

The fields of robot grasping and dexterous manipulation have received increased attention over the last years, as robots have already started to interact with their surroundings and assist humans in the execution of dexterous tasks. Since the human hand is considered to be Nature's most dexterous end-effector, the prospect of replicating human dexterity has motivated roboticists to follow bio-inspired approaches [21, 26, 61, 62]. This is due to the fact that the human hand is the most dexterous end-effector known, consisting of 29 joints, 27 bones, and more than 123 ligaments that are actuated by more than 30 muscles in a synergistic fashion [31]. One of the most important joints in human hand is the metacarpophalangeal joint (MCP), which allows the fingers to execute both adduction/abduction and flexion/extension motions, thus increasing the dexterity of the overall system. Moreover the human thumb's MCP joint is responsible for the opposition which is a powerful motion of the human hand operation [31].

1.2 Objectives

The focus in this thesis is on enhancing the robotic hand's performance that will facilitate the execution of various grasping and in-hand manipulation tasks, by employing less actuators

without losing dexterity [6]. More specifically, the objectives are,

1. Design and develop a minimal actuation mechanism to combine various motions, similarly to the MCP joint.
2. Design and develop an adaptive anthropomorphic robot hand.
3. Employ less number of actuators so that the robot hand's complexity is reduced, the developed hand is lightweight, and the fabrication remains significantly low.
4. Inherit the grasping capabilities of adaptive devices.
5. Perform various in-hand manipulation tasks with the robot hand, e.g., object rolling, finger interdigitation, and equilibrium point manipulation.

1.3 Contributions

The contribution of this thesis is fourfold. First, we design and develop a tendon-driven actuation mechanism for adaptive monolithic robotic fingers that extends their dexterous performance. The actuation mechanism design is minimal and modular, while it makes use of simple mechanical elements. We investigate the performance of compliant monolithic fingers that make use of flexure joints based on elastomer material (urethane rubber), yet our suggested actuation mechanism can be applied to other applications. The proposed mechanism has the ability to perform concurrently flexion/extension and adduction/abduction on the MCP joint, by employing two actuators in a synergistic fashion. We present a modeling framework to compensate gravity with a torsion spring. We also provide design specification parameters for various adduction/abduction motions through a mechanism analysis. A model of the finger for performing spatial motion is discussed. Our actuation mechanism

improves the dexterous workspace and amplifies the exerted finger forces. Next, we employ the monolithic fingers to design and develop a new adaptive, humanlike robot hand that can: i) achieve selective interdigitation, switching from power grasps to pinch grasps and optimizing its robust grasping performance to specific objects and ii) execute dexterous, in-hand manipulation tasks (e.g., equilibrium point manipulation), offering an increased dexterity. Furthermore, a design optimization framework is introduced that derives the differential mechanism configuration and the differential motion of cable-driven, under-actuated, anthropomorphic robot hands. The efficiency of the proposed design and methods has been extensively validated using a wide range of experimental paradigms.

1.4 List of Publications

This thesis has resulted to 1 journal paper and 2 conference papers. All publications are currently (December 2018) under review.

Journal paper

- [1] G. P. Kontoudis, M. Liarokapis, K. G. Vamvoudakis, T. Furukawa, “An Adaptive Actuation Mechanism for Anthropomorphic Robot Hands,” 2018. (*under review*)

Conference papers

- [1] G. P. Kontoudis, M. Liarokapis, K. G. Vamvoudakis, T. Furukawa, “An Adaptive Robot Hand for Selective Interdigitation, Robust Grasping, and Dexterous, In-Hand Manipulation,” 2018. (*under review*)
- [2] G. P. Kontoudis, M. Liarokapis, K. G. Vamvoudakis, T. Furukawa, “A Modular Actuation Mechanism for Adaptive Robotic Fingers,” 2018. (*under review*)

1.5 Outline

The remainder of this thesis is organized as follows. Chapter 2 discusses the related work, Chapter 3 focuses on the design of the actuation mechanism and performs an analysis of the design constraints, Chapter 4 focuses on the design of the proposed adaptive, humanlike robot hand, Chapter 5 presents the results of the experimental validation, while Chapter 6 concludes the thesis and discusses future directions.

Chapter 2

Literature Review

In this chapter we present previous works in actuation mechanisms, robotic fingers, and robot hands. We give particular emphasis on adaptive robot hands that are closely related with our work.

2.1 Robotic Fingers

In [54], the authors proposed a double active universal joint (DAUJ) that was implemented with gear transmission and two actuators. Their focus was on in-pipe inspection systems and robotic fingers with pin joints. The work of [44], presented the UBH 3 that was equipped with tendon-driven, spring loaded pin joints on fingers. The robot hand was able to perform grasping and in-hand manipulation by using 16 actuators. The authors in [63] introduced an anthropomorphic robotic finger with pin joints that employed a biomimetic tendon-routing system and a pneumatic actuation scheme. Their objective was to develop a robotic finger that has identical function with human fingers. In [38], the authors proposed a compliant robotic finger design that integrates passive parallel compliance. Their design combines elastomer materials along with a specific structure that performs as a variable stiffness compliant joint towards improving the stability in grasping and manipulation. In [57], presented a rotational elastic joint for underactuated robotic fingers. Their design is monolithic and the joint is implemented with an embedded spiral torsion spring. The flexion/extension analysis

for robotic fingers with pin joints and flexure joints has been studied in [7, 50] and in [51] respectively.

Monolithic structures can significantly simplify the manufacturing process and reduce the manufacturing cost, as they require a single step process [37]. They also lack of wear, backlash, and friction which impacts to minimal detrimental effect [29]. In the work of [1] presented a methodology to design compliant mechanisms, based on the topology optimization homogenization method [5]. However, when the employed material is flexible, then the rigid body assumption is not guaranteed for all geometries. In [30] presented the pseudo-rigid-body model to design compliant mechanisms with flexure elements that identifies which flexural segments act as rigid bodies. A soft monolithic finger was presented in [49]. The authors investigated various types of flexure joints and fabricated the finger by employing the Fused Deposition Modeling (FDM).

2.2 Anthropomorphic Robot Hands

Traditionally, the problems of robot grasping and dexterous manipulation have been addressed using rigid, fully actuated, multi-fingered robot hands [12, 32, 45]. These devices are typically heavy, expensive, difficult to build and maintain, and they rely on sophisticated sensing elements and complicated control laws in order to operate in unstructured and dynamic environments. Recently, a new class of adaptive robot hands was introduced [2, 3, 13, 16, 22, 27, 28, 36, 42, 59, 60] that attempts to revolutionize the fields of robot grasping and manipulation, by simplifying the extraction of robust grasps under object pose uncertainties and the execution of dexterous, in-hand manipulation tasks. These hands are considered adaptive, since they are equipped with flexure or spring loaded pin joints, under-actuated fingers, and differential mechanisms. Differential mechanisms allow the hands to

conform with unknown object's shape without any means of feedback. In [23, 48, 52] the authors developed adaptive robot hands that can perform in-hand manipulation tasks. The authors in [20] studied in-hand manipulation using a robot hand with a single actuator that exploits extrinsic resources.

Regarding anthropomorphism of robot motion, a previous study [35, 40] investigated the affinity in structure and motion of robotic hands and the human hand. This study proposed a methodology for the quantification of robot hands anthropomorphism. The human-identical model is compared in two different stages with various robot hands by employing computational geometry and set theory methods to derive a comprehensive index of anthropomorphism that can be used for design optimization purposes.

For the control of hand posture, a Neuroscience study [56] revealed that during grasping actions, a coupling/higher-level coordination in the human hand fingers' motion exists. This study concluded that the first two principal component vectors, of the grasp covariance matrix account for approximately 84% of the variance of the total human hand grasping actions. The particular finding inspired new designs of robot hands and control schemes that simplify the execution of everyday grasps. In [9, 13] the authors presented several synergy-based robotic hands for humanlike grasping, but each actuator could trigger only a single synergy. This means that the weight of the robotic hand in all cases was increased, while the final force transmitted to the fingers for grasping and manipulation was restricted. In [17], the authors focused on bringing the aforementioned statistical neuroscience study in robotics, introducing new representative robot hand grasping strategies called eigengrasps. More precisely, the authors used a dimensionality reduction technique in order to represent the robot hand motion capabilities in low-d manifolds, where the control is relaxed and the task execution is simplified. The derived strategies account again for most of the grasping actions variance and are useful for solving online grasp planning problems.

Adaptive hands can be developed either with flexure joints (elastic joints) or with spring loaded pin joints. The elastic elements in the finger structures are typically used for a passive implementation of the finger extension. Regarding adaptive hand designs, in [52] the authors proposed the i-HY hand, an adaptive robot hand that was developed specifically for in-hand manipulation. In [62] the authors proposed a theoretical framework for designing anthropomorphic robot hands for robust grasping tasks. More specifically they proposed underactuated fingers fingers to implement the human finger adaptability. The work of [24] proposed the Pisa/IIT SoftHand 2 that implements two actuators to enhance the grasping and manipulation capabilities. The design make use of a single cable that connects the two actuators and the robot hand achieved rolling of various objects. Chen et al. [14] proposed an an optimization methodology, named mechanically realizable manifolds, to search for grasping synergies and achieve stable grasping given the kinematics of an underactuated robot hand and a set of possible grasps. They also proposed an adaptive robot hand based on their methodology. In [11], the authors presented a finger with an alternative tendon-driven actuation design based on shape memory alloys (SMA) instead of cables. The proposed finger, has 2 degrees of freedom (DoF¹) for the MCP joint, yet these motions were independent, while 1 SMA was responsible for the flexion/extension. Thus, only 1 SMA contributed to the power transmission in grasping. In [25], the authors analyzed a planar and a spherical mechanism for fingers abduction in human-like robot hands. These mechanisms can achieve various differential motions for adduction/abduction, according to specific requirements. However, these mechanisms do not transfer power to the fingers and actuation is required for not only the abduction, but also for the adduction in order to maintain the robot hand in its natural position. In [55], the MCP joint ranges of motion of the human hand for adduction/abduction were presented. These ranges were different for each finger of the human hand, making their implementation in under-actuated mechanisms challenging.

¹We will use DoF for singular and plural forms.

2.3 Summary

Many research groups have presented excellent works on adaptive robot hands. However, only recent works in [24, 52] introduced adaptive robot hands that can perform in-hand manipulation. Our work blends novel actuation mechanisms to augment the grasping capabilities and to extend the dexterity of adaptive robot hands by keeping less actuators. We are particularly interested in anthropomorphic adaptive robot hands that maintain the fraction of actuators over fingers below one, and yet achieve dexterous various in-hand manipulation tasks.

Chapter 3

Finger Design

In this chapter, we present the design of the adaptive robot finger and we describe the tendon-driven actuation mechanism that allows the finger to perform both flexion/extension (F/E) and adduction/abduction (A/A). Next, we present the modeling framework to compensate gravity with mechanical elements. The actuation mechanism analysis is provided to specify design parameters for various applications. The fabrication procedure of the anthropomorphic, compliant robotic fingers is also discussed.

3.1 Actuation Mechanism Design

The finger structure is monolithic and consists of an elastic body (made out of urethane rubber) and plastic parts, as presented in Figure 3.1. The robotic finger is actuated by tendons in a similar fashion with the human hand. The distal, middle, and proximal phalanges are connected with flexure joints. Portions of the finger with reduced width are designed to implement these flexure joints. The MCP spring loaded pin joint is responsible for the A/A. Besides the MCP joint's motion, the design is also modular since the fingers are attached in the base frame with a single bolt-nut set.

The actuation mechanism utilizes two independent tendon-routing systems to actuate the finger, as shown in Figure 3.2. We equip the proposed actuation mechanism with moment arm pulleys to drive the tendon-routing system through a specific path. On this path, the

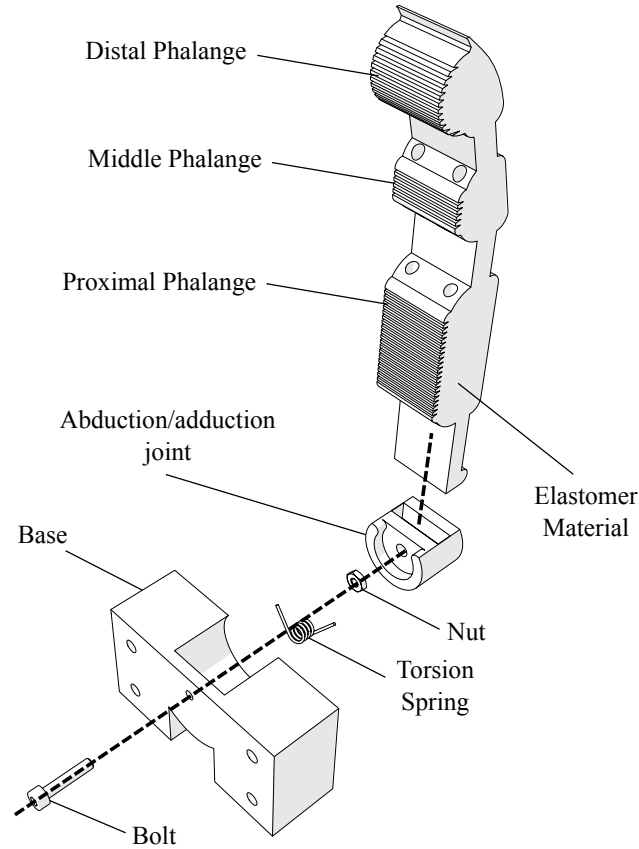


Figure 3.1: An exploded view of the finger's 3D model design. The finger is compliant as it employs elastomer material to implement the flexure joints. The design modularity is reflected by using a single bolt-nut set to connect to the palm.

line of action of the applied force does not pass from the center of the pulley's axis of rotation. Therefore, the forces transferred through the tendon-routing system, create a moment that rotates the finger. Each tendon is responsible for a different motion. The tendon with ending point at the central anchor (first actuator) is only responsible for the F/E motion of the finger. The tendon with ending point at the right side anchor point (second actuator) triggers initially the A/A motion and then contributes to the F/E of the finger. This twofold contribution in motion and force transmission lies in the design choice to place the right side anchor point at the distal phalange and not to the middle or the proximal phalange. In case

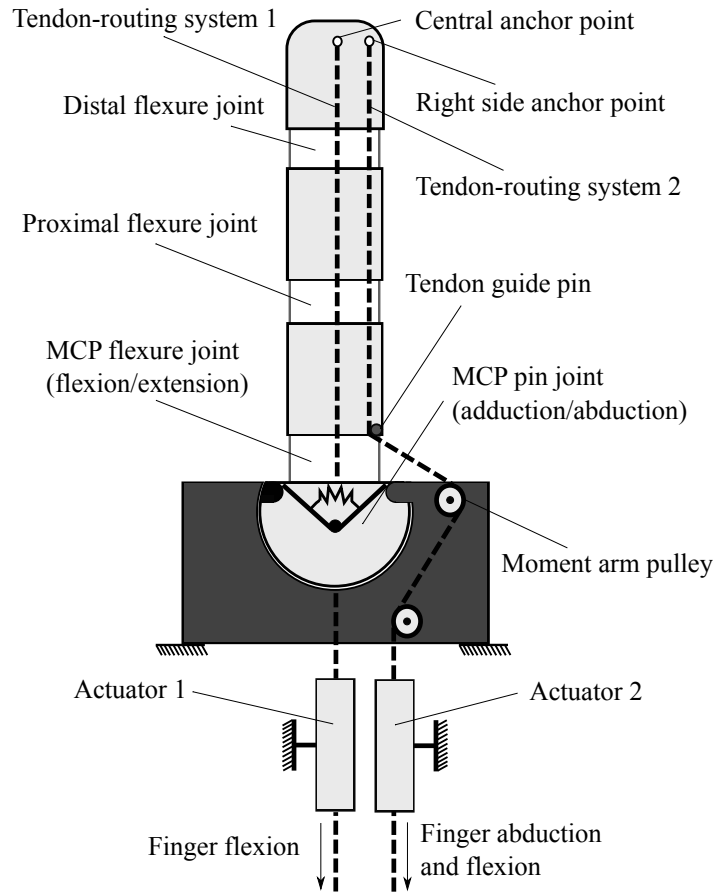


Figure 3.2: The actuation mechanism that allows for F/E and A/A concurrently. This finger operates with clockwise motion. For counterclockwise motion, the right side anchor point needs to be swiftd on the left side. For bidirectional abduction, the central anchor point needs to be placed on the left side of the finger.

of concurrent tendon actuation the F/E is the dominant motion.

The selection of anchor points for each separate tendon-routing system is determined according to the desired finger motion. One can notice that from the human hand neutral position, the index abduction moves oppositely from the ring and pinky abduction motions. The abduction motion from the natural position of the middle finger can be neglected since it is relatively small. On the other hand, the thumb motion includes bidirectional A/A. Therefore, for an anthropomorphic hand design we should be able to produce three different types of finger abductions. For this purpose, we employ right-side anchor points for

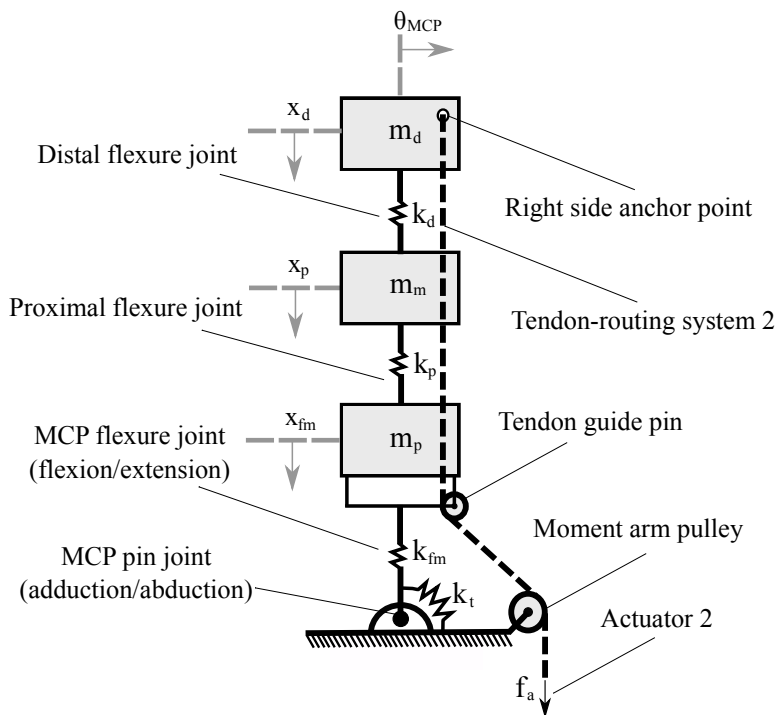


Figure 3.3: The mechanical model of a compliant finger that achieves a clockwise rotation. The flexure joints were modeled as a spring-damper and each phalange as a mass. The flexion/extension of the DIP, PIP, and MCP joints reflects the x_d , x_p , and x_{fm} motions respectively, while the adduction/abduction occurs towards the θ rotational direction.

clockwise motion, left-side anchor points for counterclockwise motion, and both-sides anchor points for bidirectional rotation. In case we pursue single side rotation, central anchor points utilization is imposed to actuate the finger F/E movements.

3.2 Rigid Body Modeling

In Figure 3.3, a mechanical model of the compliant robotic finger is presented. We employ a spring-mass system to model the finger and its compliant flexure joints. When no contact occurs and since the finger makes use of two tendon routing systems, it eliminates by design nonlinearities of the elastomer material such as twisting and lateral bending (bounding

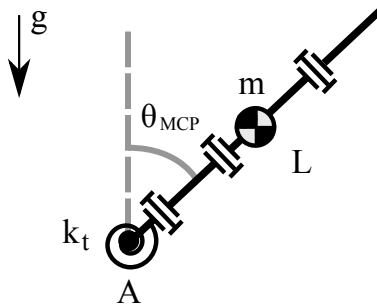


Figure 3.4: A model of the robotic finger for computing the gravity compensation with a torsion spring.

out-of-plane motion). This makes our assumption valid for the flexure joint modeling, as discussed in [33]. The mechanical model consists of discrete mass nodes distributed throughout the finger. The masses m_d , m_m , m_p represent the distal, the middle, and the proximal phalange masses respectively. The stiffness k_d , k_p , k_{fm} correspond to the distal interphalangeal (DIP), the proximal interphalangeal (PIP), and the MCP flexure joints respectively. The spring with stiffness k_t models the torsion spring. The dashed line is the tendon that triggers first the adduction/abduction and then contributes to the flexion/extension motion. The force f_a , at the end of the tendon routing system, is the actuator force.

The finger is maintained to its rest position with a torsion spring, that also mechanically implements the passive adduction motion. The stiffness of the torsion spring should be precisely selected. In case of an extremely soft torsion spring, the finger might be sensitive to gravity or to external forces and might also struggle to maintain stable contact points with the object. On the other hand, a highly stiff torsion spring, comparing with the elastomer material stiffness, makes the MCP joint work exclusively as a revolute joint for the finger's flexion motion. Therefore, the actuation mechanism is analyzed to compensate the gravity as a statically balanced mechanism, similarly to [18, 53], yet with a torsion spring. By

employing the Euler's equation of motion

$$\begin{aligned}\Sigma M_A &= I_A \ddot{\theta}_{\text{MCP}} \\ M_A^{fk} - M_A^{fm} &= m \left(\frac{L}{2}\right)^2 \ddot{\theta}_{\text{MCP}} \\ k_t \theta_{\text{MCP}} - mg \frac{L}{2} \sin \theta_{\text{MCP}} &= m \left(\frac{L}{2}\right)^2 \ddot{\theta}_{\text{MCP}},\end{aligned}\tag{3.1}$$

where M_A^{fk} is the restoring moment of the torsion spring about the point A, M_A^{fm} is the moment of the concentrated mass due to the gravity about the point A, I_A is the mass moment of inertia of a massless rod about the point A, θ_{MCP} is the abduction angle, $\ddot{\theta}_{\text{MCP}}$ is the angular acceleration, m is the concentrated mass, g is the gravity acceleration, L is the finger length, and k_t is the stiffness of the torsion spring as depicted in Figure 3.4.

For the statically balanced case the system becomes homogeneous and its angular acceleration is $\ddot{\theta}_{\text{MCP}} = 0$, so from Equation (3.1) the torsion spring stiffness results to

$$k_t(\theta_{\text{MCP}}) = mg \frac{L \sin \theta_{\text{MCP}}}{2 \theta_{\text{MCP}}}.$$

Next, by considering the small angle approximation, i.e. $\sin(\theta_{\text{MCP}}) \approx \theta_{\text{MCP}}$, the minimum torsion spring stiffness to compensate gravity yields,

$$k_{t,\min} = \frac{mgL}{2}.$$

The stiffness of the flexure joints is related with the transmitted force to the finger, so the flexure joint stiffness k_d, k_p, k_{fm} needs to be high. On the other hand, the stiffness of the torsion spring k_t needs to be stiff enough to compensate gravity and successfully rebound the finger to its rest position. Therefore, we consider that the stiffness of the flexure joints is much larger than the stiffness of the torsion spring $k_d, k_p, k_{fm} > k_{t,\min}$. Since we analyze

the worst case scenario for the torsion spring, the flexure joints will also compensate gravity. To this end, the adaptive finger will compensate gravity even when the gravitational forces are not aligned.

3.3 Actuation Mechanism Modeling and Analysis

We employ a spring-mass system to model the finger and its compliant flexure joints. When no contact occurs, and since the finger makes use of two tendon routing systems, it eliminates by design nonlinearities of the elastomer material such as twisting and lateral bending (bounding out-of-plane motion). This makes our assumption valid for the flexure joint modeling, as discussed in [33]. The mechanical model consists of discrete mass nodes distributed throughout the finger. The masses m_d , m_m , m_p represent the distal, the middle, and the proximal phalange masses respectively. The stiffness k_d , k_p , k_{fm} correspond to the DIP, PIP, and MCP flexure joints respectively.

Since our focus is on the A/A motion, we need to narrow down the problem and determine the corresponding design characteristics. For our analysis we consider that the stiffness of the flexure joints is much larger than the stiffness of the torsion spring $k_d, k_p, k_{fm} > k_t$. The stiffness of the flexure joints affects the forces that can be transmitted to the finger, so the flexure joint stiffness k_d, k_p, k_{fm} needs to be high. On the other hand, the torsion spring k_t needs to be stiff enough to compensate gravity and successfully rebound the finger to its rest position. These two factors are in accordance with the aforementioned stiffness selection.

The key idea underlying the actuation mechanism is that, by selecting various moment arm pulley positions we will be able to achieve different maximum abduction angles as presented in Figure 3.5. That is a dependent motion problem with constraints the tendon length and the datum. The datum is imposed by the moment arm pulley's position. The maximum

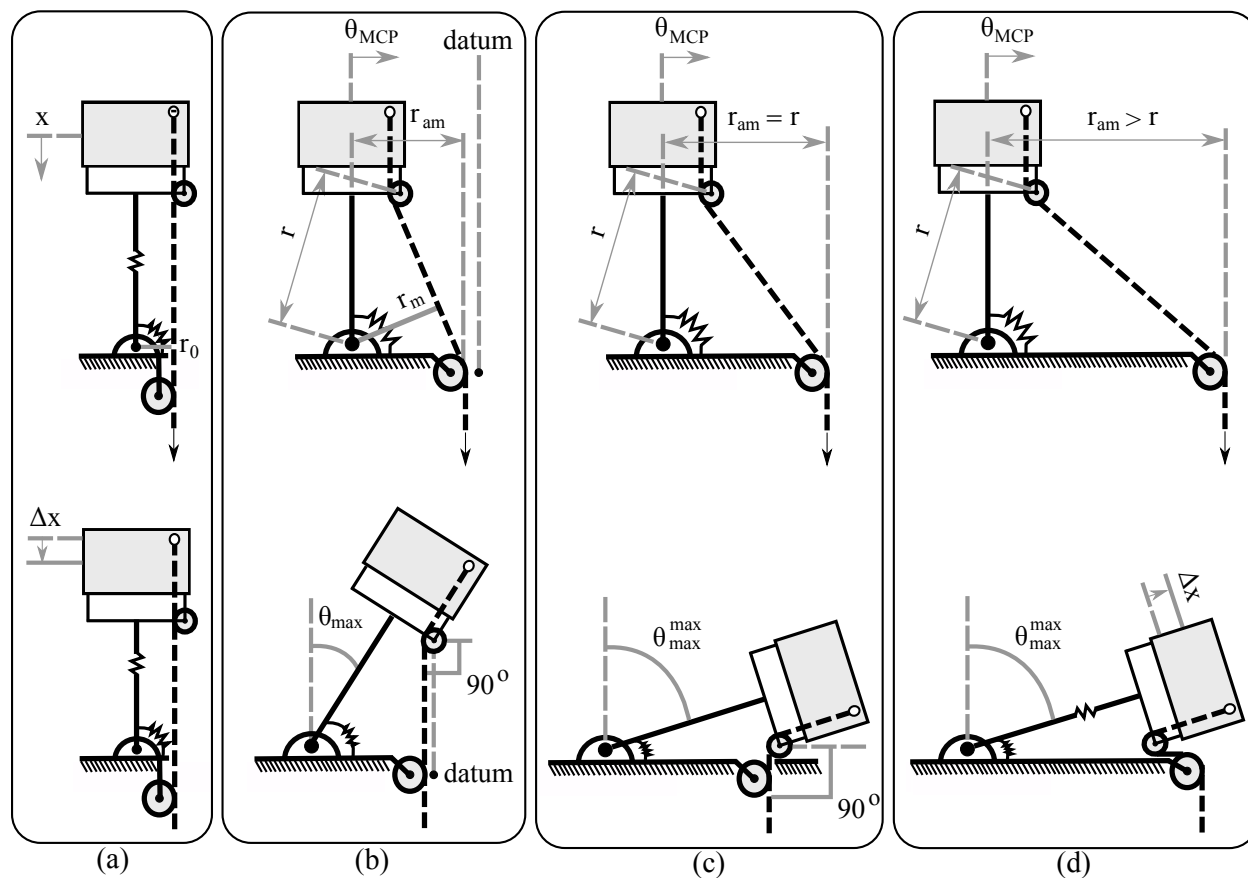


Figure 3.5: The actuation mechanism in various configurations. Different design choices with respect to the moment arm pulley position, produce various abduction motions. (a) The moment arm pulley is perpendicular with the tendon guide pin. (b) The moment arm pulley is in an intermediate position. (c) The distance from the joint axis of rotation to the moment arm pulley r_{am} matches the radius length r . (d) The distance from the joint axis of rotation to the moment arm pulley r_{am} is higher than the radius length r .

abduction angle occurs when the finger pulley reach the datum.

The actuator that is responsible for the A/A first triggers the abduction, until it reaches its higher possible abduction angle, and then contributes to the F/E motion as depicted in the lower part of Figure 3.5. When the moment arm pulley is by design perpendicular with the tendon guide pin, then the mechanism will trigger only perpendicular motion Δx , because the moment arm r_0 is relatively small, as shown in Subfigure 3.5(a). In case that we select the position of the moment arm pulley at a horizontal distance r_{am} , the moment arm will be

increased to r_m . Therefore, the mechanism will be abducted until its datum point at θ_{\max} , as depicted in Subfigure 3.5(b). Next, for the maximum abduction angle θ_{\max}^{\max} the moment arm pulley should be placed at a distance $r_{\text{am}} = r$, as presented in Subfigure 3.5(c). The last possible choice is to place the moment arm pulley at a distance $r_{\text{am}} > r$ where the finger will first reach its maximum abduction θ_{\max}^{\max} , but then it will be subject to tensile stress with a Δx deformation as shown in Subfigure 3.5(d).

We tackle two problems. First, we specify the design parameters in order to achieve the desired abduction angle θ_{\max} in the mechanism. Second, we determine the transferred force to the finger after the friction losses that are induced by the reconfiguration at the maximum abduction angle θ_{\max} . For the A/A motion analysis, the actuation mechanism model is depicted in Figure 3.6. The joint length is the l_1 and the length l_2 is the finger pulley distance. The actuation mechanism has an internal angle α that is invariant of the actuator displacement and depends only on the mechanism design. The abduction angles that the actuation mechanism achieves range $\theta_{\text{MCP}} \in [-\frac{\pi}{2} + \alpha, \frac{\pi}{2} - \alpha]$ for bidirectional abduction. Since our analysis deals with clockwise abduction, the mechanism achieves a range $\theta_{\text{MCP}} \in [0, \frac{\pi}{2} - \alpha]$, yet the exact same analysis applies for counterclockwise and bidirectional abduction. The angle β is formed by the perpendicular line of the link and the tendon. The length l_3 is the distance from the tendon guide pin to the moment arm pulley. The distance from the abduction joint axis of rotation to the tendon guide pin is illustrated by r . As the mechanism performs abduction the distance r_{am} remains constant. On the other hand, the perpendicular distance from the abduction joint axis to the guide pin decreases to l_4 , when the mechanism arrives at its maximum abduction angle.

The variable that imposes the moment arm is also responsible for the maximum abduction angle. That is, the length l_3 at the initial configuration without any actuator displacement. Given the finger design characteristics l_1, l_2 and the desired maximum abduction angle θ_{\max} ,

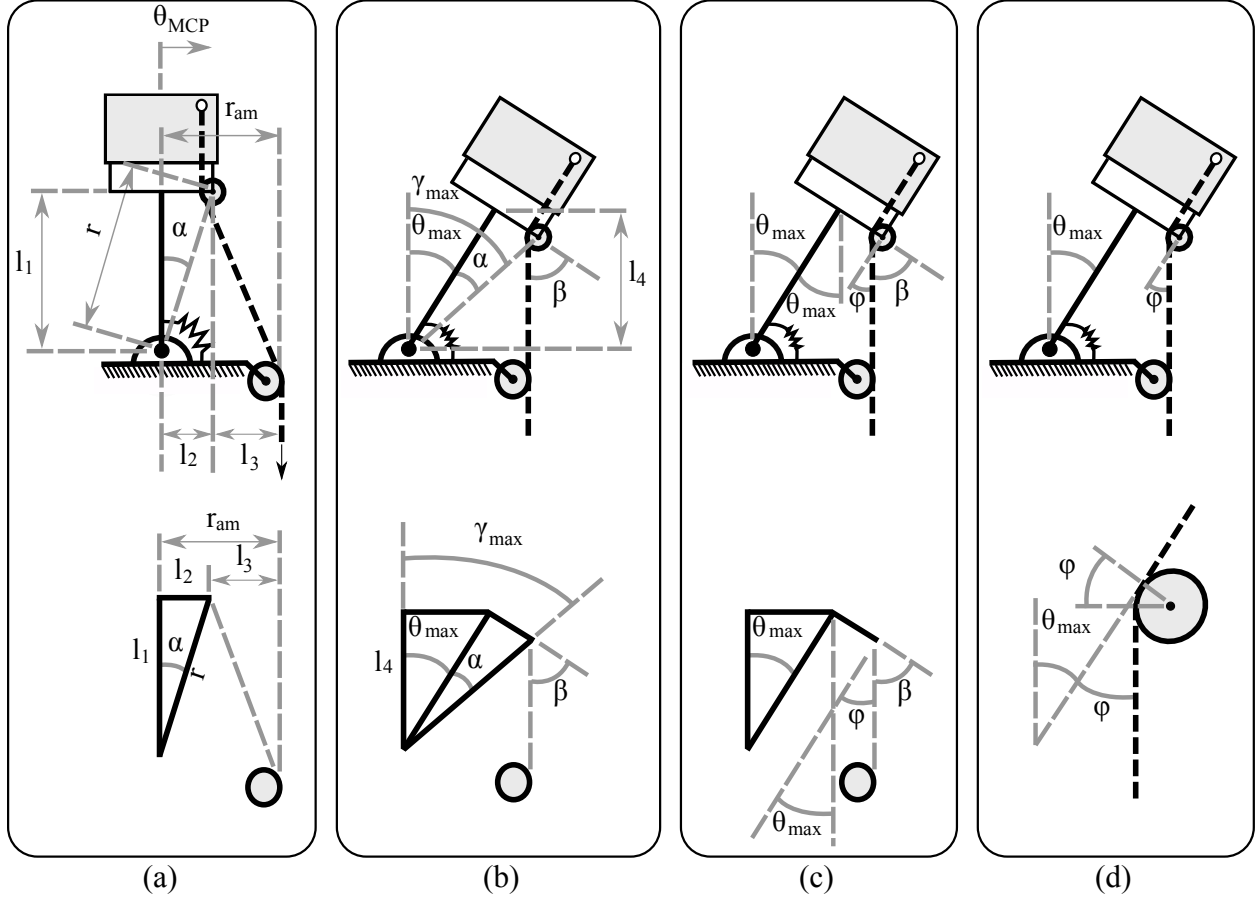


Figure 3.6: The actuation mechanism model at the initial and at the maximum abduction configuration. (a) The mechanism characteristics at the initial configuration. (b) The mechanism characteristics at the maximum abduction angle. (c) The mechanism characteristics at the maximum abduction angle. (d) The mechanism characteristics focused on the tendon guide pin at the maximum abduction angle.

we need to justify the distance of the length l_3 . At the maximum abduction angle we have $\theta_{\max} = \gamma_{\max} - \alpha$. Then, from the initial configuration we obtain,

$$\alpha = \arctan\left(\frac{l_2}{l_1}\right). \quad (3.2)$$

Next, we find that the maximum abduction angle γ_{\max} as follows,

$$\sin \gamma_{\max} = \sin(\theta_{\max} + \alpha) = \frac{r_{\text{am}}}{r}. \quad (3.3)$$

Given that $r_{\text{am}} = l_2 + l_3$, the Equation (3.3) takes the form of,

$$l_3 = \sin(\theta_{\max} + \alpha)r - l_2. \quad (3.4)$$

Considering that at the initial configuration the length $r = \sqrt{l_1^2 + l_2^2}$, we express the desired length l_3 exclusively as a function of the maximum abduction angle θ_{\max} and the finger design characteristics l_1, l_2 from Equation (3.4) as follows,

$$l_3 = \sin \left[\theta_{\max} + \arctan \left(\frac{l_2}{l_1} \right) \right] \left(\sqrt{l_1^2 + l_2^2} \right) - l_2.$$

For the second problem we consider the Euler-Eytelwein equation $T_{\text{load}} = T_{\text{hold}}e^{\mu\phi}$. As the finger rotates, the abduction angle θ increases, which results to the reduction of β angle. Note that ϕ and β are complementary, which yields $\phi = 90 - \beta$ as shown in Subfigure 3.6(c). Therefore, we need to justify the maximum angle ϕ , at the maximum abduction angle θ_{\max} , to account for the maximum friction exerted forces. The key observation is that for the proposed mechanism the ϕ angle, at the maximum finger abduction, is the same with θ_{\max} , as shown in Subfigure 3.6(d). Therefore, the available force for the flexion at the maximum abduction position yields $T_{\text{hold}} = \frac{T_{\text{load}}}{e^{\mu\theta_{\max}}}$.

The modeling of tendon-driven underactuated fingers has been studied for the planar case in [4, 8, 46]. However, the proposed mechanism establishes spatial motions and thus another

model is required. The kinematics of the coupling finger yields,

$$\mathbf{J}_a^\top \Delta \boldsymbol{\theta} = \mathbf{r}_a \Delta \boldsymbol{\theta}_{am}, \quad (3.5)$$

where $\mathbf{J}_a \in \mathbb{R}^{n \times m}$ is the actuation Jacobian with n denoting the number of DoF and m the number of actuation modes, $\boldsymbol{\theta} \in \mathbb{R}^n$ is the finger configuration, $\mathbf{r}_a \in \mathbb{R}^{m \times m}$ is the diagonal matrix of the actuator pulley radii values, and $\boldsymbol{\theta}_{am} \in \mathbb{R}^m$ is the actuation mode angle vector.

The number of actuators is not equivalent with the number of actuation modes, as combined operation or even individual actuator triggering results to different finger motions. More specifically, the abduction actuator enforces the MCP abduction, but when both actuators operate then the finger is flexed. In our analysis, we consider four actuation modes. The first two actuation modes are dedicated for individual actuator operation that reflect to either flexion or abduction. The third actuation mode is correlated with the abduction actuator after the maximum abduction angle is achieved, resulting to finger flexion. The fourth actuation mode concerns simultaneous motion of the tendon-routing systems, that reflect to finger flexion. In this way, we can control the adaptive finger in every possible scenario. The actuation Jacobian has the form of,

$$\mathbf{J}_a = \begin{bmatrix} r_d & 0 & r_d & r_d \\ r_p & 0 & r_p & r_p \\ r_{fm} & 0 & r_{fm} & r_{fm} \\ 0 & r_{am} & 0 & 0 \end{bmatrix},$$

where r_d , r_p , r_{fm} , and r_{am} are the pulley radii of the DIP, PIP, flexion MCP, and abduction MCP joints respectively. The finger configuration for every actuation mode is given by $\boldsymbol{\theta} = [\theta_d \ \theta_p \ \theta_{fm} \ \theta_{MCP}]^\top$ as presented in Figure 3.7. For simplicity we consider the actuator

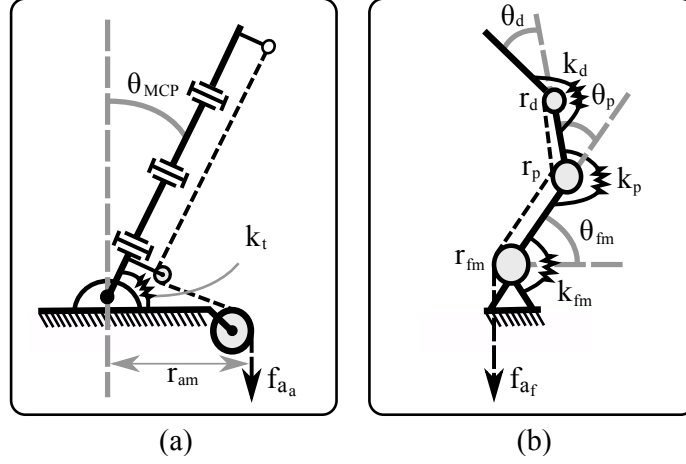


Figure 3.7: The finger model for spatial motion. (a) The abduction θ_{MCP} is performed from the abduction actuator f_{a_a} . (b) The flexion is occurred either from the flexion actuator f_{a_f} , or from the combined motion of both actuators, or from the abduction actuator when $\theta_{MCP} > \theta_{max}$.

pulley values as $\mathbf{r}_a = \mathbf{I}$, where \mathbf{I} is an identity matrix of appropriate dimensions. The actuation mode angle vector is $\boldsymbol{\theta}_{am} = [\theta_1 \ \theta_{2a} \ \theta_{2f} \ \theta_3]^T$, where θ_1 is the individual operation of actuator 1, θ_3 is the combined actuators motion, and θ_{2a} , θ_{2f} represent the individual operation of the actuator 2 for abduction and flexion respectively that yields,

$$\theta_2 = \begin{cases} \theta_{2a}, & \text{if } \theta_{MCP} \leq \theta_{max} \\ \theta_{2f}, & \text{otherwise.} \end{cases}.$$

Therefore, from Equation (3.5) we obtain the finger motion for every actuation mode,

$$\Delta\theta_1 = \Delta\theta_{2f} = \Delta\theta_3 = r_d\Delta\theta_d + r_p\Delta\theta_p + r_{fm}\Delta\theta_{fm},$$

$$\Delta\theta_{2a} = r_{am}\Delta\theta_{MCP}.$$

Next, we present a static balance analysis to obtain the required tendon force for every joint.

We assume that there are no external disturbances to the finger, i.e. $\mathbf{f}_e = \mathbf{0}$, similarly to [46].

Then, the static balance equation is given by,

$$-\mathbf{K}\Delta\boldsymbol{\theta} + \mathbf{J}_a^T \mathbf{f}_a = 0, \quad (3.6)$$

and $f_a \in \mathbb{R}^+$ the tendon force. Note, that the Equation (3.6) cannot blend various actuation modes and thus the actuation Jacobian is reduced to $\mathbf{J}_a \in \mathbb{R}^n$. The stiffness matrix for the actuation modes that impose flexion motions has the form of $\mathbf{K}_1 = \mathbf{K}_3 = \mathbf{K}_4 = \text{diag}(k_d, k_p, k_{fm}, 0)$, and for the abduction actuation mode $\mathbf{K}_2 = \text{diag}(0, 0, 0, k_t)$. The actuation Jacobians for the flexion actuation mode are $\mathbf{J}_{a_1} = \mathbf{J}_{a_3} = \mathbf{J}_{a_4} = [r_d \ r_p \ r_{fm} \ 0]$, and for the abduction actuation mode $\mathbf{J}_{a_2} = [0 \ 0 \ 0 \ r_{am}]$. Therefore, the required tendon force for the flexion f_{a_f} and for the abduction f_{a_a} without any disturbance yields,

$$f_{a_f} = \frac{k_d \Delta\theta_d}{r_d} = \frac{k_p \Delta\theta_p}{r_p} = \frac{k_{fm} \Delta\theta_{fm}}{r_{fm}}, \quad (3.7)$$

$$f_{a_a} = \frac{k_t \Delta\theta_{MCP}}{r_{am}}. \quad (3.8)$$

For the worst case scenario that occurs when the finger is flexed at the maximum abduction angle the tendon force is further reduced to $f_{a_f}^{\max} = \frac{f_{a_f}}{e^{\mu\theta_{\max}}}$, and $f_{a_a}^{\max} = \frac{f_{a_a}}{e^{\mu\theta_{\max}}}$.

3.4 Developed Finger

The fabrication procedure and the adaptive finger are presented in Figure 3.8. The flexure joints are corner-filletted as they are more bending-compliant and they also develop lower stresses [43]. We employed the Hybrid Deposition Manufacturing (HDM) technique [47] using two different molds. More specifically, we use a reusable mold (blue), a rotating base (purple), and a sacrificial mold (black) as presented in Subfigure 3.8(a). The sacrificial mold

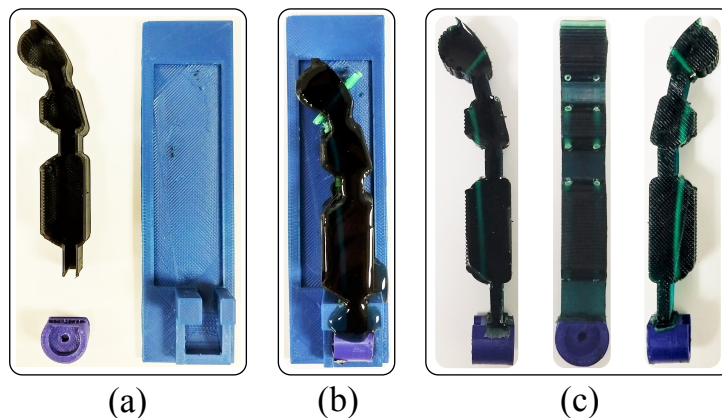


Figure 3.8: The fabrication process of the developed finger. (a) The reusable mold in blue, the rotating base in purple, and the sacrificial mold in black. (b) The elastomer material at the curing phase. (c) Side views and front view of the fabricated finger.

has holes to penetrate the low friction tubes (green parts) as shown in Subfigure 3.8(b). Then, the reusable mold accommodates the sacrificial mold and the rotating base to prevent elastomer leakage as depicted in Subfigure 3.8(c). The rotating base has a special geometry with rounded corners to guarantee a robust interlink of the two bodies [19].

The finger is a monolithic structure that consists of urethane rubber (shore hardness 80 A, Smooth-On - PMC 780) and plastic parts (e.g., tendon routing tubes). We utilize the low-friction tubes to eliminate the friction in the tendon-routing system and 3D printed ABS material for the rotating base to ensure the structure robustness. Since the finger is unibody, we implement geometrically the flexure joints with 6 mm width for the PIP and the DIP joints, and 4.5 mm width for the MCP joint (making the MCP joint more compliant). The design is anthropomorphic, as it optimizes the humanlikeness metrics described in [40]. We exploit the material deformability to enlarge the contact surfaces [15]. The torsion spring has stiffness $k_t = 0.5 \text{ N.mm/deg}$, to mechanically rebound the finger at its initial position. We employed exclusively off-the-shelf materials that reduce the cost and expedite the fabrication process. The finger is considered lightweight as it weighs only 25 g. The design incorporates a modular finger that can be easily replaced.

3.5 Summary

In this chapter, we presented and analyzed the actuation mechanism for adduction/abduction. We show that the position of the moment arm pulley can be determined for desired abduction angles. Moreover, we introduced the actuation modes of the proposed mechanism to describe all possible finger motions. Next, the fabrication process of the developed finger is presented. We employed exclusively off-the-shelf materials and the HDM technique.

Chapter 4

Robot Hand Design

In this chapter, we present the design of the adaptive robot hand with two parallel differential mechanisms based on the Whiffletree. Next, we discuss an optimization framework to derive the differential mechanism configuration and compute the differential motion. Then, we describe the fabrication process of the robot hand and we list its characteristics.

4.1 Differential Mechanism Design

We equip the particular robot hand with the proposed actuation system by using 4 tendon-routing systems and 2 parallel differential mechanisms based on Whiffletree as presented in Figure 4.1. More specifically, we employ one differential mechanism as a single tendon-routing system for the F/E of the four digits and similarly the other differential mechanism as the second tendon-routing system for the A/A of the three digits. The rest two tendon-routing systems are dedicated to the thumb abduction and the thumb adduction. It is to be noted that when the tendon-routing systems of the thumb are simultaneously actuated then F/E is occurred to the thumb. Ranges of adduction/abduction motion varies depending on the finger [55]. In order to tune the motion of every finger, we can either select torsion springs of certain stiffness levels, or we can modify the structure of the differential mechanism.

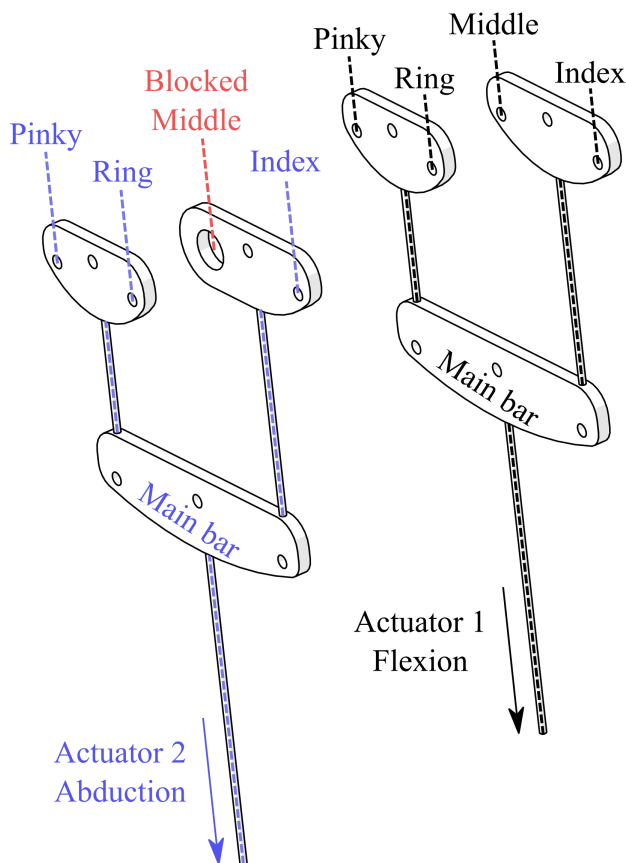


Figure 4.1: The two parallel differential mechanisms based on the Whiffletree. The differential mechanism comprises of three bars. One bar to actuate the index and middle fingers, one bar to actuate the ring and pinky fingers, and the main bar to connect the actuator with the two bars. The first tendon-routing system is responsible for the F/E of the four fingers and the second tendon-routing system performs A/A on three fingers.

4.2 Design Optimization

In this chapter we discuss the differential mechanism configuration scheme using static optimization techniques [39] and we provide relations for various differential motions.

We modify the differential mechanism's parameters as a means to optimize the A/A motion of the MCP joint for every finger. For the A/A we employ a selectively lockable differential mechanism that has the ability to vary its displacement when fingers are locked. For our analysis, we assume that tendons remain vertical and the input force of the differential

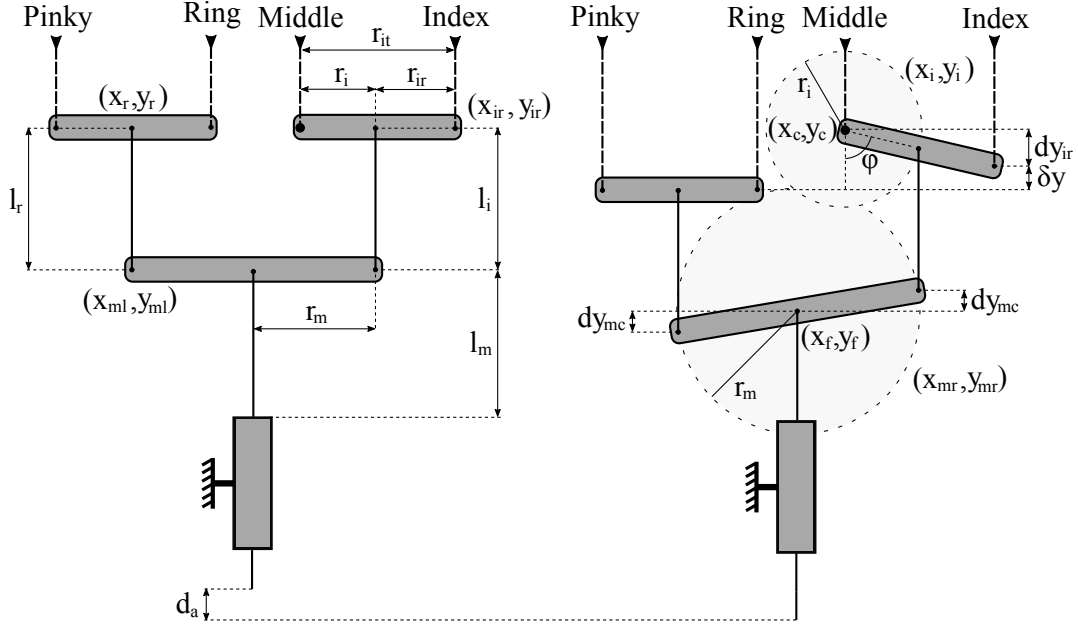


Figure 4.2: The design optimization parameters of the proposed differential mechanism. The two top bars are responsible for the index and the ring-pinky A/A motions. The blocked finger is depicted as solid black circle. The main bar connects the 2 top bars with the actuator. The attachment points are located in the center of all bars.

mechanism F_a is equally distributed to the remaining 3 digits $F_a^i = F_a^r = F_a^p = \frac{F_a}{3}$, where F_a^i , F_a^r , F_a^p are the output forces of the differential mechanism for the index, ring, and pinky fingers respectively. Since the middle finger is blocked, the bar that corresponds to the index finger rotates circularly around its center as illustrated in Figure 4.2. The mechanism consists of 3 bars and a single actuator for the A/A of the four digits. The two top bars are responsible for the index and the ring-pinky A/A motions. The middle finger's motion is blocked to its rest position. The main bar connects the 2 top bars with the actuator. We select the attachment points to be in the middle of all bars, but this selection can vary depending on the differential motion requirements. To this end, the total displacement of the actuator gives us the position of the attachment point.

The formulation of the static optimization problem yields the differential mechanism configuration is defined as follows,

$$\underset{x_i, x_{mr}, y_i, y_{mr}}{\text{minimize}} \quad D_{mi}(x_i, x_{mr}, y_i, y_{mr}) \quad (4.1)$$

$$\text{subject to:} \quad x_{mr}^2 + (y_{mr} - y_f)^2 = r_m^2, \quad (4.2)$$

$$(x_i - x_c)^2 + (y_i - y_c)^2 = r_i^2, \quad (4.3)$$

$$x_{mr} - x_i = 0, \quad (4.4)$$

$$y_{mr} - y_i - l_i = 0, \quad (4.5)$$

where $x_{mr}, y_{mr} \in \mathbb{R}$ are the coordinates of the right edge of the main bar, $x_i, y_i \in \mathbb{R}$ are the coordinates of the cable attachment point of the index bar, $x_c, y_c \in \mathbb{R}$ are the coordinates of the constrained connection of the middle finger, $l_i \in \mathbb{R}^+$ is the length of the cable that connects the main bar with the index bar, $r_m, r_i \in \mathbb{R}^+$ are the radii of the main bar rotation and the index bar rotation respectively, $d_a \in \mathbb{R}^+$ is the displacement of the actuator, and $D_{mi} \in \mathbb{R}^+$ is the distance between the edge of the main bar and the index bar attachment point as shown in Figure 4.2. In (4.2) we describe the constraint of the main bar in circular motion, in (4.3) we provide the constraint of the index bar in circular motion, in (4.4) we introduce the constraint of the assumption about exclusively vertical motion of the tendons, and in (4.5) we provide the constraint of uniform tendon length (i.e. zero deformation). We define the distance D_{mi} of (4.1) as,

$$D_{mi}(x_i, x_{mr}, y_i, y_{mr}) = \|m - i\|^2, \quad (4.6)$$

where m, i are the Cartesian points that we want to justify, and $\|\cdot\|$ denotes the Euclidean norm. The vertical tangent line that connects the m, i points is the optimal solution. The coordinates at the middle finger's constrained connection can be easily obtained from the structure of the differential mechanism as, $x_c = r_m - r_i \in \mathbb{R}^+$ and, $y_c = l_m + l_i \in \mathbb{R}^+$,

where $l_m \in \mathbb{R}^+$ is the length of the cable that connects the actuator with the main bar. Moreover, the coordinates at the main bar's attachment point are given as, $x_f = 0$ and, $y_f = l_m - d_a \in \mathbb{R}^+$.

Next, we obtain the differential mechanism configuration. The main bar's slope produces a perpendicular distance from its right edge to the center, $dy_{mc} = y_{mr} - y_f \in \mathbb{R}^+$. Since the main bar attachment point is placed at its center, dy_{mc} is symmetric, and thus the same in both edges. The y -coordinate of the main bar's left edge is given as, $y_{ml} = y_f - dy_{mc} \in \mathbb{R}^+$. Then, we calculate the ring bar y -coordinate which remains horizontal, because the attachment point is located at the ring bar's center. The ring bar y -coordinate yields from, $y_r = y_{ml} + l_r \in \mathbb{R}^+$, where $l_r \in \mathbb{R}^+$ is the length of the cable that connects the main bar with the ring bar. For the calculation of the differential motion, we also need to determine the y -coordinate at the right edge of the index bar. Therefore, we calculate the index bar slope with the Y-axis, $\cos(\phi) = \frac{y_c - y_i}{r_i}$. Next, we obtain the perpendicular distance $r_{ir} \in \mathbb{R}$ of the index bar's right edge towards the fixed point of the middle finger, $dy_{ir} = (r_i + r_{ir}) \cos(\phi) \in \mathbb{R}^+$. The y -coordinate of the right edge at the index bar yields from, $y_{ir} = y_c - dy_{ir} \in \mathbb{R}^+$. Finally, we are able to calculate the differential motion, $\delta y = (y_{ir} - y_r) \in \mathbb{R}$.

The proposed differential mechanism configuration scheme solves a challenging kinematics problem in a minimal way, by employing static optimization techniques [39]. The framework consists of only 4 variables, that are x_i , x_{mr} , y_i , and y_{mr} , and 4 constraints in (4.2), (4.3), (4.4), and (4.5) to derive the differential motion δy . The rest parameters can be easily obtained with geometric relations.

For a given displacement of the actuator, the bar associated with the ring and pinky motion displays larger displacement than the index bar as shown in Figure 4.3. We also observe that the index bar length reduction results to increased differential displacement δy_i for the same actuator displacement d_{ai} . Since the actuator displacement cannot exceed the length of the

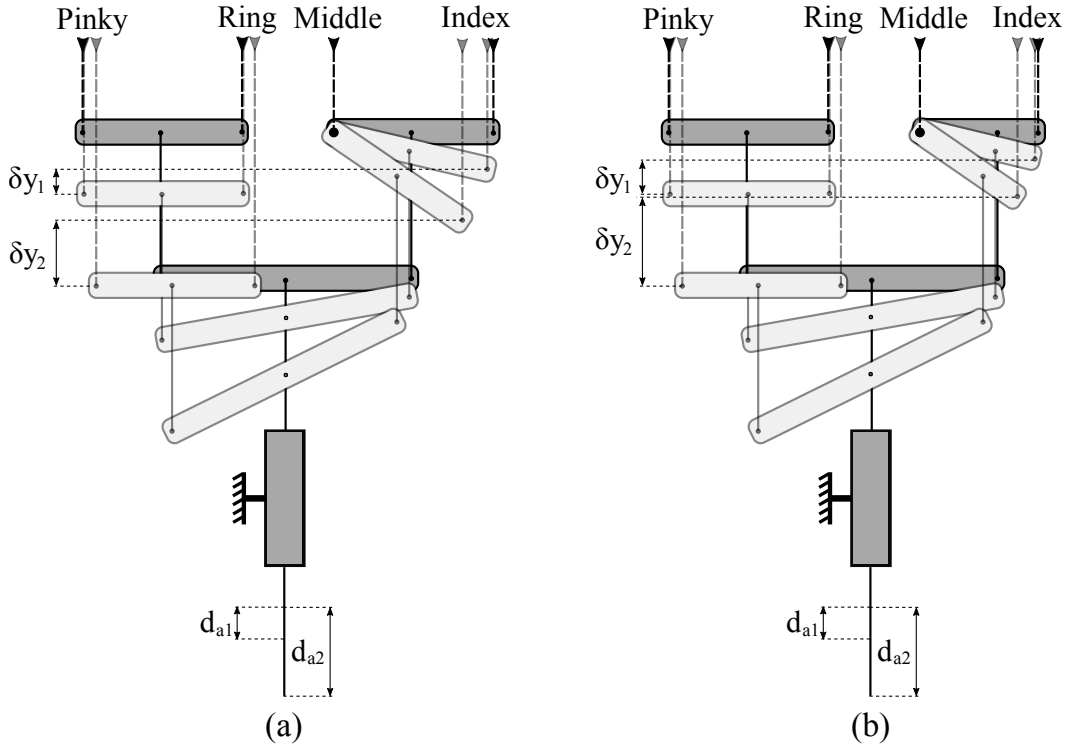


Figure 4.3: The alteration of differential motion according to the design characteristics. The length reduction on the blocked index bar generates larger differential motion (δy_i) for the same actuator displacement (d_{ai}). (a) The 2 top bars have the same length. (b) The bar that is related with index digit's motion is shorter than the other top (ring-pinky) bar.

cable that connects the actuator with the main bar we set $d_a^{\max} \leq l_m \in \mathbb{R}^+$. Next, we exploit the generated discrepancy in the displacement of the bars to actuate different A/A motions on the remaining 3 digits. In our study, we only alter the length of the index bar. Other design parameters, such as the main bar's relative length, can be taken into consideration, depending on the device requirements and the task specifications.

4.3 Fabrication Process

For the fabrication process of the proposed adaptive robot hand, we employed exclusively off-the-shelf materials that can be easily found in hardware stores around the world. The an-

Table 4.1: Finger Dimensions of Robot Hand

<i>Finger</i>	<i>Weight</i>	<i>Length</i>	<i>Breadth</i>	<i>Width</i>	<i>Abduction</i>
Index	25 g	88 mm	16.2 mm	15 mm	25°
Middle	25 g	98 mm	16.2 mm	15 mm	Fixed
Ring	25 g	95 mm	16.2 mm	15 mm	-24°
Pinky	20 g	76 mm	16.2 mm	15 mm	-28°
Thumb	20 g	68 mm	16.2 mm	15 mm	$\pm 165^\circ$

thropomorphic fingers are monolithic and they are fabricated with urethane rubber (Smooth-On - PMC 780) of shore hardness 80 A using the Hybrid Deposition Manufacturing (HDM) technique [47]. We list their characteristic in Table 4.1. The total weight of each finger is 25 g. The link lengths of the fingers and the hand dimensions follow the anthropocentric models described in [10].

The kinematics of the fingers depend on the width of the the proximal IP (PIP), the distal IP (DIP), and the MCP flexure joint. We select the width of the joints experimentally, by following a medical test. This test is developed in medicine for human hand surgeries. The test provides a quick and robust validation of the human hand function after operations. In Figure 4.4 we demonstrate the Kapandji test, which follows two steps [31].

1. The thumb's fingertip must be able to contact with the MCP base frames of the index, middle, ring, and pinky fingers.
2. The thumb's fingertip must be able to contact the index and pinky fingertips, without any flexion on the PIP and DIP joints.

In Table 4.2, the radius of each joint is listed. Note that the thumb performs F/E to the DIP and PIP joints and the middle finger performs only F/E. After the selection of the finger widths we employ the smooth curvature model [51] to derive the stiffness of each joint as shown in Table 4.3. Then, we relate the stiffness of the flexure joints with the stiffness

Table 4.2: Finger Joint Radii

<i>Finger</i>	Index	Middle	Ring	Pinky	Thumb
<i>Radius DIP - F/E</i>	10.00 mm	10.00 mm	10.00 mm	10.00 mm	1.00 mm
<i>Radius PIP - F/E</i>	10.00 mm	10.00 mm	10.00 mm	10.00 mm	1.25 mm
<i>Radius MCP - F/E</i>	12.50 mm	12.50 mm	12.50 mm	12.50 mm	-
<i>Radius MCP - A/A</i>	15.00 mm	-	15.00 mm	15.00 mm	28.50 mm

of the torsion spring. More specifically, the torsion spring needs to be characterized by enough stiffness to mechanically rebound to its initial position and to concurrently counteract gravity. On the other hand, it should be soft enough to allow the A/A when the tendon shifts, otherwise F/E dominates and A/A diminishes. The resulting torsion spring stiffness follows the analysis in Chapter 3.3. The MCP joint of the thumb performs A/A without the need of the a torsion spring, as we employ side anchor points for the tendon-routing systems.

Next, we compute the required tendon force for each actuator by utilizing the (3.7), (3.8). The desired flexion angles of each joint are 90° for the DIP joint, 100° for the PIP joint, and 80° for the MCP joint, as presented in [35]. Yet, due to palm restrictions the maximum attained PIP joint angle is 40° . Also, we employ by design a DIP rest angle of 20° from [31]. To this end the DIP joint operates from 20° to 90° , i.e. 70° . Therefore, the required force for the flexion of the four fingers yields, $f_{a_f, \text{total}} = f_{a_f, \text{index}} + f_{a_f, \text{middle}} + f_{a_f, \text{ring}} + f_{a_f, \text{pinky}} = 70$ N, where $f_{a_f, i} = f_{a_f, i, \text{DIP}} + f_{a_f, i, \text{PIP}} + f_{a_f, i, \text{MCP}}$. Similarly, the required tendon force for the abduction of the three fingers is, $f_{a_a, \text{total}} = f_{a_a, \text{index}} + f_{a_a, \text{ring}} + f_{a_a, \text{pinky}} = 8$ N, where $f_{a_a, i} = f_{a_a, i, \text{MCP}}$. We equip the robot hand with 2 Dynamixel RX-28 servo motors with torque $T_m = 2.8$ Nm at 12V and outer shaft diameter $D_m = 0.0025$ m for the F/E and A/A. Then we place a pulley to the outer shaft with diameter $D_p = 0.0500$ m. The resulting tendon force of each actuator is $f_a = 112$ N. Since both actuators are contributing to the F/E, the four fingers can easily perform full flexion. It is to be noted that we use significantly higher torque motors to ensure robust grasping and dexterous in-hand manipulation.

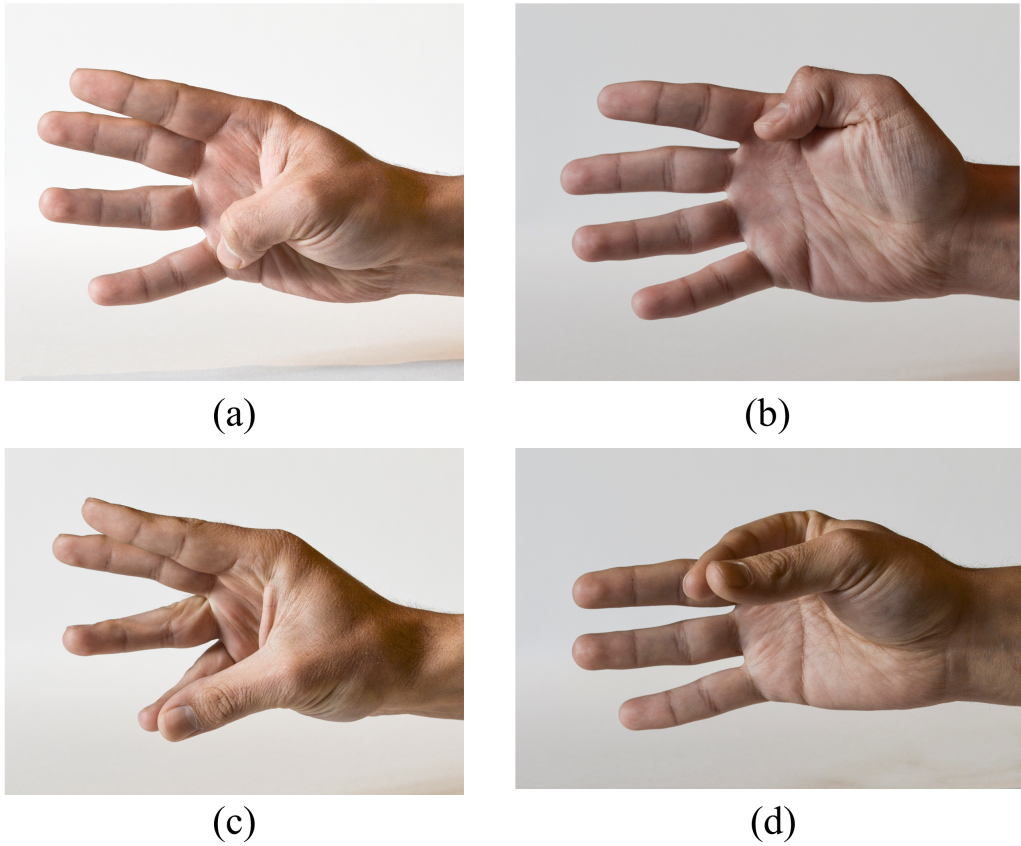


Figure 4.4: The representation of the Kapandji test (a) Thumb fingertip in contact with the pinky MCP base frame. (b) Thumb fingertip in contact with the index MCP base frame. (c) Thumb fingertip in contact with the pinky fingertip and without any flexion on the PIP and DIP joints. (d) Thumb fingertip in contact with the index fingertip and without any flexion on the PIP and DIP joints.

In Table 4.4, the characteristics of the robot hand are presented. The robot hand was exclusively fabricated from 3D printed ABS material. The hand length (HL) and the hand breadth (HB) are anthropomorphic according to [10], and the weight is 650 g. The hand

Table 4.3: Finger Joint Rotational Stiffness

<i>Finger</i>	Index	Middle	Ring	Pinky	Thumb
<i>Stiffness DIP - F/E</i>	1.25 $\frac{\text{N.mm}}{\text{deg}}$				
<i>Stiffness PIP - F/E</i>	1.25 $\frac{\text{N.mm}}{\text{deg}}$	1.25 $\frac{\text{N.mm}}{\text{deg}}$	1.25 $\frac{\text{N.mm}}{\text{deg}}$	1.25 $\frac{\text{N.mm}}{\text{deg}}$	0.65 $\frac{\text{N.mm}}{\text{deg}}$
<i>Stiffness MCP - F/E</i>	0.65 $\frac{\text{N.mm}}{\text{deg}}$	0.65 $\frac{\text{N.mm}}{\text{deg}}$	0.65 $\frac{\text{N.mm}}{\text{deg}}$	0.65 $\frac{\text{N.mm}}{\text{deg}}$	-
<i>Stiffness MCP - A/A</i>	0.50 $\frac{\text{N.mm}}{\text{deg}}$	0.50 $\frac{\text{N.mm}}{\text{deg}}$	0.50 $\frac{\text{N.mm}}{\text{deg}}$	0.50 $\frac{\text{N.mm}}{\text{deg}}$	Bidirectional

Table 4.4: Robot Hand Characteristics

<i>Dimensions</i>	HL = 185 mm, HB = 90 mm
<i>Weight</i>	650 gr, with motors
<i>Motors</i>	4 Dynamixel RX-28, 2.8 Nm at 12V
<i>Software</i>	ROS
<i>Materials</i>	3D printed ABS; Smooth-On PMC-780 (urethane rubber)
<i>Availability</i>	Open-source
<i>Cost</i>	\$ 1,000
<i>Motions</i>	Thumb: CW & CCW A/A, F/E; Index: CW A/A, F/E; Middle: F/E; Ring: CCW A/A, F/E; Pinky: CCW A/A, F/E

accommodates 4 Dynamixel RX-28 servo motors with available torque 2.8 Nm at 12 V. The actuation scheme provides a variety of motions to the robot hand. More specifically, for a right hand, the thumb achieves clockwise (CW) and counterclockwise (CCW) A/A, while also F/E, the index CW A/A and F/E, the ring and the pinky CCW A/A and F/E, and the middle F/E. The design is open-source and can be found in [41].

4.4 Summary

In this chapter, we presented the differential mechanisms of the adaptive robot hand. The flexion of the four fingers is implemented with a regular Whiffletree. For the abduction motion we employed a variation of the Whiffletree that constraints the motion of the middle finger. Also, we discussed an optimization framework to derive the differential mechanism configuration and the differential motion of the fingers. Then, we described the fabrication process of the robot hand that was based on additive manufacturing techniques and off-the-shelf materials.

Chapter 5

Results and Experiments

In this chapter, we assess the rigid-body-assumption with a finite element method (FEM). Then, we evaluate the efficiency of the actuation mechanism and we compute the workspace of the robotic finger. Next, we analyze the grasping forces to investigate the force exertion capabilities of the finger and assure that the joint preserves its position when it is abducted. We also perform a force comparison with a finger at the fully abducted position. Furthermore, we validate the efficacy of the proposed finger design by performing two set of experiments that include the implementation of various finger postures and the manipulation of an object. Next, we evaluate the efficiency of the actuation mechanism. We analyze the grasping forces to investigate the force exertion capabilities of the finger and we assure that the joint preserves its position when it is abducted. We also perform a force comparison with a finger at the fully abducted position. Furthermore, we validate the efficacy of the proposed finger design by performing two set of experiments that include the implementation of various finger postures and the manipulation of an object.

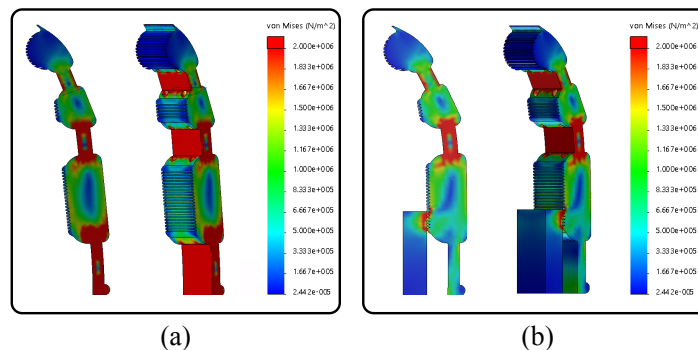


Figure 5.1: Flexion response of the monolithic adaptive finger with FEM. (a) Finger flexed in the free space. (b) Finger flexed while in contact with an obstacle that constraints the MCP flexure joint motion.

5.1 Finger Experiments

5.1.1 Finite Element Method

We investigate the rigid-body-assumption through a FEM approach [64]. The adaptive finger was studied with a standard/implicit FEM in SolidWorks 2017 (Dassault Systems). During the simulation, the elastomer material was assumed to be uniform and solid, while its properties were assigned according to the manufacturer [58]. The stress distribution is presented in Figure 5.1. The finger geometry was not altered and the obstacle was considered a non-deformable object (i.e. metallic). In Subfigure 5.1a, the finger is studied in the free space. The areas that collect more stress are the flexure joints. In Subfigure 5.1b, an obstacle constraints the motion of the MCP flexure joint. The obstacle has sufficiently low height to allow for potential bending of the proximal phalange. However, the stress is still distributed in the unconstrained PIP and DIP flexure joints where the flexion occurs.

The strain results of the simulation indicate that for the specific urethane rubber and given a geometry with smaller width 4.5 mm for the MCP joint and 6.0 mm for the PIP and DIP joints, the phalanges with width 16.0 mm can be modeled as rigid bodies and thus the rigid-

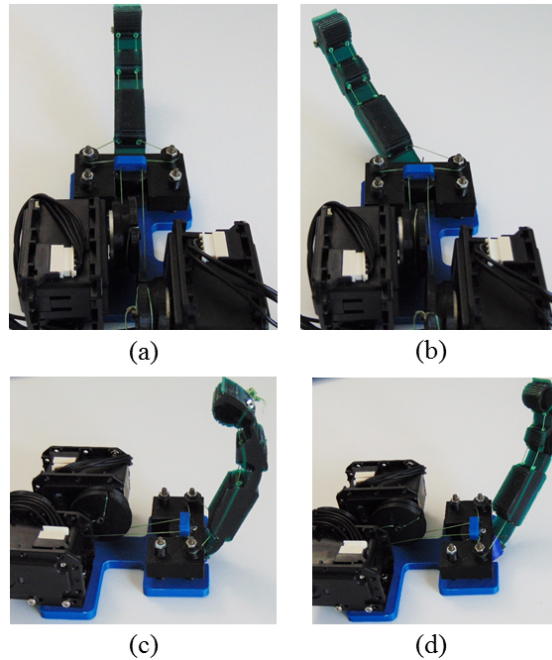


Figure 5.2: The anthropomorphic finger in various configurations. (a) Finger in the neutral (rest) position. (b) Finger abduction by using the corresponding tendon-driven system. (c) Finger flexion without any abduction. (d) Finger flexion in an abducted angle.

body-assumption is valid. It is to be noted that the finite element method was employed only for the evaluation of the rigid body assumption.

5.1.2 Finger Postures

In this subsection we perform finger posture experiments that include an individual finger flexion, an individual finger abduction, a finger flexion at the highest abduction configuration, and a finger abduction at the highest flexion configuration. The finger configurations of flexion and abduction are presented in Figure 5.2. The anthropomorphic index finger equipped with the actuation mechanism is capable of performing A/A and F/E concurrently. We are able to achieve the A/A motion of all human hand fingers. More specifically, for a left hand from the palm side view it is required, counterclockwise motion for the index

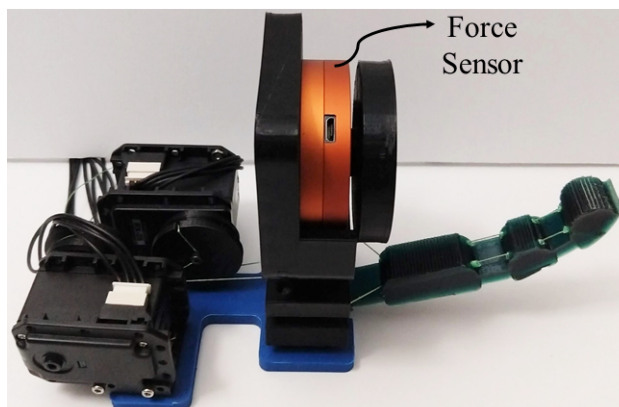


Figure 5.3: The experimental setup for measuring the finger force capabilities.

finger, clockwise motion for the ring and pinky fingers, and bidirectional motion for the thumb finger.

5.1.3 Force Exertion Capabilities

For the actuation of the two tendon-driven systems we employed 2 Dynamixel RX-28 servo motors with torque $T_m = 2.8$ Nm at 12V and outer shaft diameter $D_m = 0.0025$ m. We placed a pulley to the outer shaft with diameter $D_p = 0.0500$ m. Large enough motors were used to assure that the finger force will not be restricted by the motor performance. We gathered the fingertip exerted forces in various configurations of a single digit with the FSE1001 force sensor (Variense), as presented in Figure 5.3. Next, we measured the exerted forces that occurred for only flexion by employing both actuators. Finally, we collected the fingertip forces in fully abducted configuration by employing again both actuators.

We conducted the experiments for 20 trials. The comparison of the fingertip exerted forces in two configurations is shown in Figure 5.4. The overall mean exerted forces are illustrated on the right side with dashed line. The solid line represents the mean value at each time, while the shadowed area depicts the standard deviation. The black-gray colored area depicts

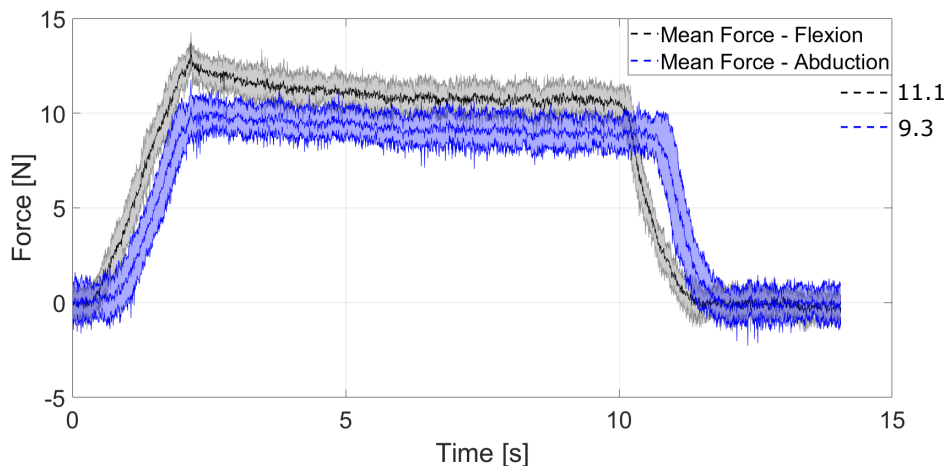


Figure 5.4: The comparison of the forces exerted by the fingertip in two different configurations. The finger reports competitive exerted forces even at fully abducted position. The decay after the overshoot represents the strain energy stored in the elastomer material of the flexure joints.

the finger forces during the simple flexion case, while the blue-light colored area depicts the finger forces during flexion in fully abducted position. The reported overall mean force for the simple flexion case is 11.1 N. The actuation mechanism not only maintains its position at the maximum abducted configuration while flexed, but it also reports a force of 9.3 N. As the finger is abducted, the achievable finger force is reduced, because of various friction losses, yet it remains significantly high. Therefore, the proposed actuation mechanism facilitates the exertion of significant finger forces even at fully abducted position, allowing the execution of robust grasping tasks.

5.1.4 Finger Workspace

The finger structure is anthropomorphic and its parameters were computed for hand length $HL = 185$ mm and hand breadth $HB = 90$ mm as discussed in [36, 65]. According to our analysis in Subsection 3.3, for desired maximum abduction angle $\theta_{\max} = 67.5^\circ$, MCP flexure joint length $l_1 = 22.00$ mm, and tendon distance $l_2 = 5.10$ mm, the required distance from

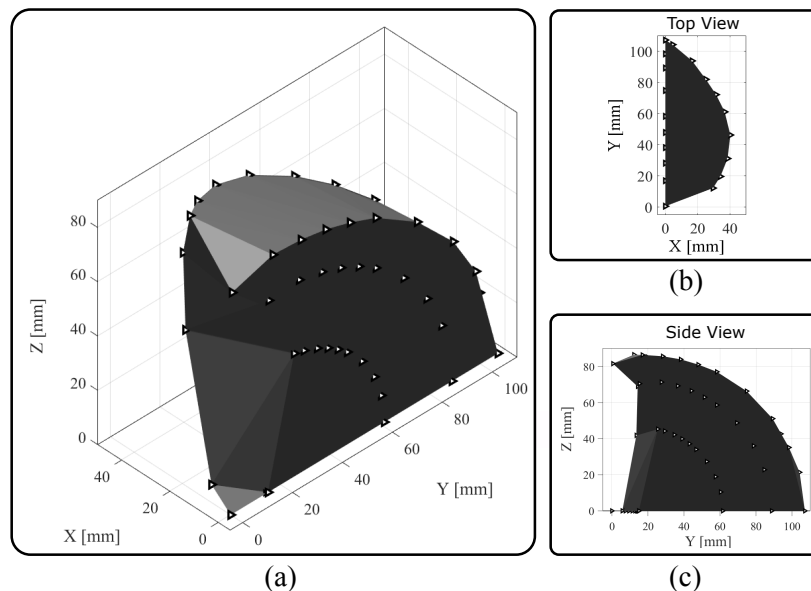


Figure 5.5: The reachable workspace of an anthropomorphic index finger. The triangles represent the position of the joints through time. (a) Perspective view. (b) The top view illustrates the finger abduction. (c) The side view depicts the finger flexion.

the abduction joint axis to the moment arm pulley is $l_3 = 17.2$ mm. The design parameters that affect the finger's motion are the moment arm pulley position, the elastomer material stiffness of the flexure joints, and the torsion spring stiffness.

We employed a standard Kinect camera (Microsoft) with 3 markers at the center of each flexure joint, 1 marker at the MCP axis of rotation for the abduction, and 1 marker at the edge of the fingertip. Then we build the workspace by connecting the 3D points with the convex hull. In Figure 5.5, the finger workspace with one side rotation is presented. The maximum angle that was attained by the MCP joint is 67.5° , thus our analysis is valid. All the intermediate configurations can be achieved by combing the 2 actuators.

The proposed actuation mechanism is amplifying the workspace, comparing to finger designs that accomplish only flexion/extension. This workspace extension will allow the execution of dexterous manipulation tasks.

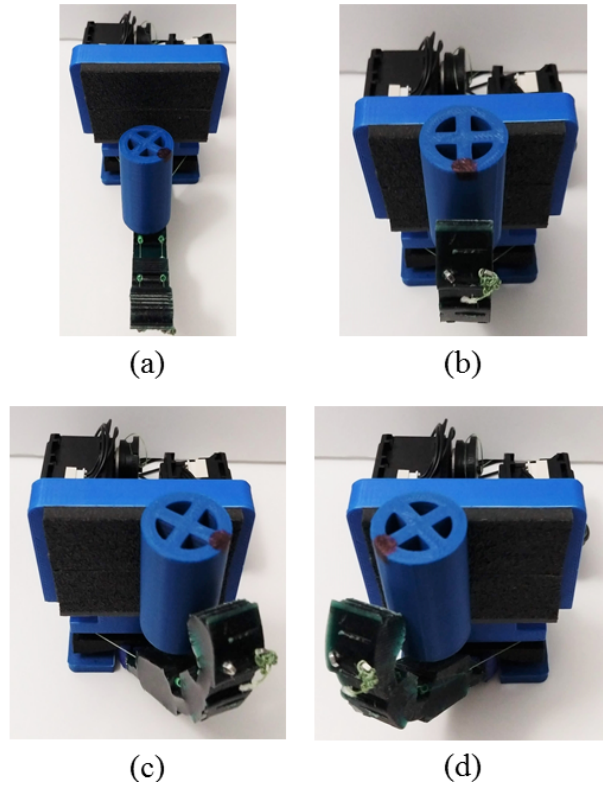


Figure 5.6: The anthropomorphic finger performing a manipulation task. (a) The adaptive finger with the cylindrical object. (b) Initial grasping position. (c) Rolling clockwise 45° . (d) Rolling counterclockwise 90° .

5.1.5 Finger Grasping and Manipulation Capabilities

For the finger grasping and manipulation experiments we used a cylindrical object. The object was fabricated with ABS 3D printed material, it has diameter $D = 25$ mm, and length $h = 50$ mm. The grasping and manipulation experiments are depicted in Figure 5.6. First, the finger and a fixed surface are used to perform a robust grasping action. Then, the finger rolls the object bidirectionally from 0° to -45° , from -45° to 45° , and from -45° to 0° . The rolling did not cause any object slip as it successfully returns at its initial position, that is indicated by a black mark on the object. This experiment reveals the grasping and manipulation capabilities of a single bidirectional adaptive finger, equipped with the proposed actuation mechanism.

5.2 Hand Experiments

5.2.1 Hand Postures and Gestures

We perform experiments with the developed robot hand to examine its anthropomorphic characteristics. In the first row of images of Figure 5.7, all the possible robot hand grasping postures and gestures are presented, while in the second row of images of Figure 5.7, we present the results of the Kapandji test [31]. It can be easily noticed that the fingertip of the thumb is able to contact the fingertips of the index and the pinky fingers, as well as their base frames, thus the Kapandji test was successful.

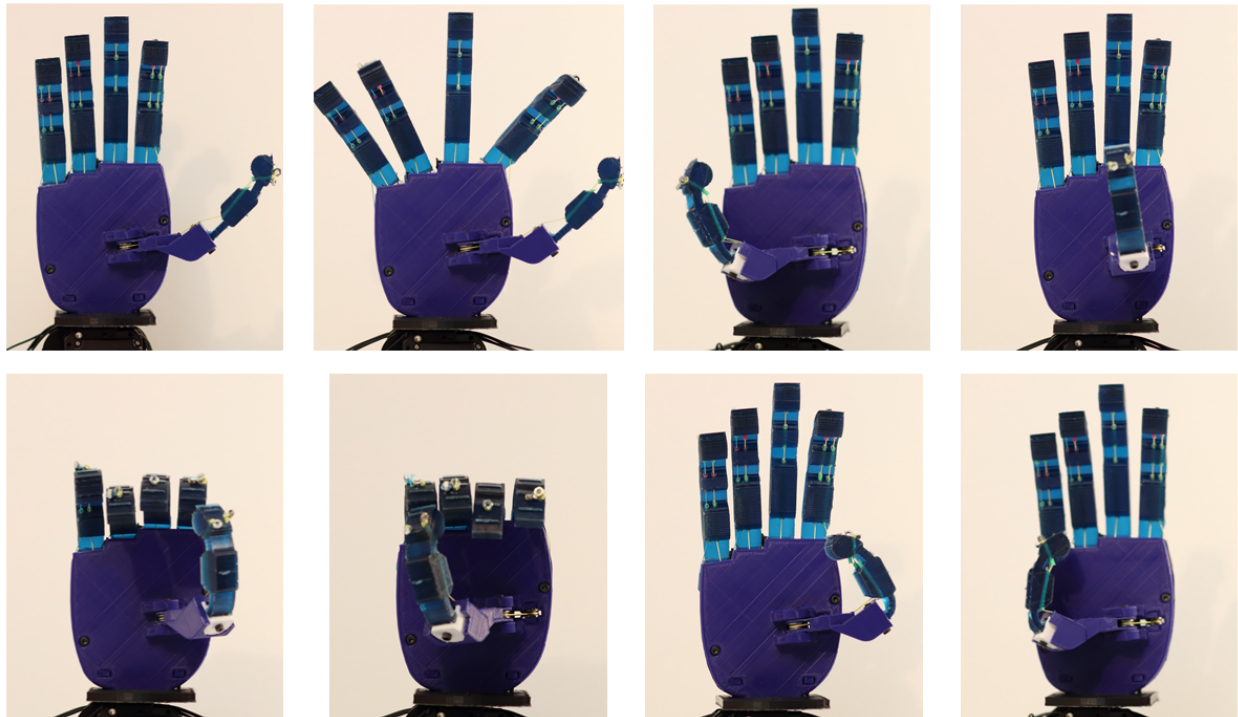


Figure 5.7: Grasping postures and gestures executed by the proposed adaptive robot hand. The A/A capabilities are depicted in the first row. The second row of images shows the implementation of the Kapandji test.

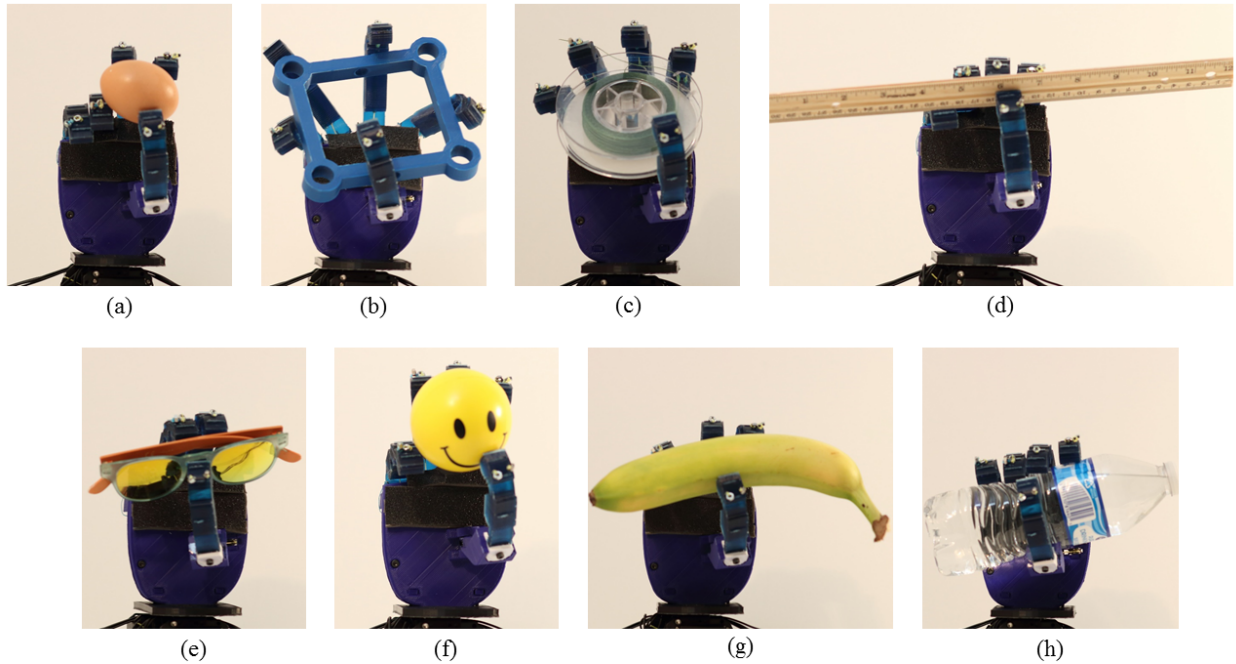


Figure 5.8: The proposed adaptive robot hand while performing grasping experiments with various everyday life objects. More precisely, the grasps involve a) an egg, b) a large rectangular object, c) a plastic cylindrical object, d) a ruler, e) a pair of sunglasses, f) a small plastic ball, g) a banana, and h) a bottle of water.

5.2.2 Grasping Everyday Life Objects

In order to experimentally validate the efficiency of the proposed adaptive robot hand and assess its grasping capabilities, we chose to conduct a wide range of experiments involving a series of everyday objects such as an egg, a 3d printed rectangular shape, a plastic cylindrical shape, a ruler, a pair of sunglasses, a small plastic ball, a banana and bottle of water. Representative grasps with the examined set of objects are presented in Figure 5.8. It is evident that the underactuation and the structural compliance of the proposed adaptive robot hand allow it to grasp and handle delicate objects like the raw egg and the pair of sunglasses without breaking them.

5.2.3 Dexterous Manipulation

The proposed adaptive, humanlike robot hand is capable of executing not only robust grasps but also dexterous, in-hand manipulation tasks using only two actuators. In particular, the hand is able to perform equilibrium point manipulation motions as well as finger gaiting motions. An example of an equilibrium point manipulation task executed with a small plastic ball is depicted in Figure 5.9.

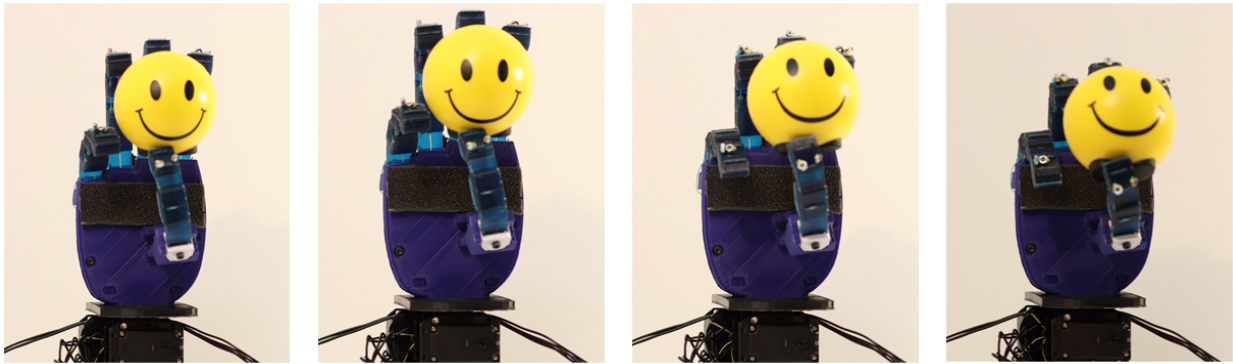


Figure 5.9: An equilibrium point manipulation experiment executed with the proposed robot hand. The robot hand successfully grasps a spherical object and then performs rolling of the object. Yet, the rolling is not simple and results also to equilibrium point motion, which is one of the most challenging dexterous manipulation tasks.

5.3 Summary

In this chapter, we validated the efficacy of the proposed design with simulations and various experiments. First, we validated the rigid body assumption with a FE analysis, that reveals stress concentration primarily on the flexure joints. Then, we computed the reachable workspace of fabricated finger. The derived workspace matches exactly the analysis in Chapter 3.3 regarding the moment arm pulley position for specific abduction angles. Then, we computed the finger exerted forces for exclusively finger flexion and at the extreme ab-

duction angle. We showed that the decrease in exerted forces is significantly low, which allow for robust grasping actions even at extreme finger configurations. Next, we performed a rolling experiment with a single finger. The object was rolled 90° without any slip.

We continue our experiments with the adaptive robot hand. First, we demonstrated the possible configurations of the robot hand. Then, we successfully performed the Kapandji test. Various everyday life objects were employed for the grasping experiments. The grasping ability of the hand is increased with the abduction of the fingers, that is related with the second postural synergy. Finally, we performed an equilibrium point manipulation experiment.

Chapter 6

Conclusions and Future Work

This thesis proposed a anthropomorphic, adaptive robot hands for robust grasping and dexterous, in-hand manipulation. More precisely, we developed anthropomorphic, adaptive fingers that are equipped with an MCP joint capable of implementing flexion/extension and adduction/abduction concurrently and individually. We presented the joint's specifications and we proposed a modeling framework that compensates gravity. We also performed a mechanism analysis that derives the appropriate parameters for the implementation of various abduction configurations. A finger model was discussed that predicts the finger motion and computes the required tendon force for every actuation mode. The validity of the rigid-body-assumption was studied with a FEM approach. The exerted force results show a force range between 9.3 N to 11.6 N for the two extreme configurations, by exploiting the torque of both actuators. Moreover, the finger workspace has increased significantly, indicating an enhancement in the overall system dexterity. Next, we validated the actuation mechanism's performance by providing experimental paradigms conducted with the developed anthropomorphic, adaptive index finger. The finger achieves adduction/abduction and flexion/extension concurrently, which results to various configurations. Furthermore, the finger is able to execute both robust grasping tasks and dexterous manipulation tasks without any slip. In addition, the humanlike robot hand that is able to achieve selective interdigitation, robust grasping and dexterous, in-hand manipulation of everyday objects. The hand consists of the developed adaptive, monolithic robot fingers. Differential mechanisms are used to simplify

the actuation scheme, utilizing only two actuators for four fingers. Selective interdigitation allows the proposed adaptive robot hand to switch from power to pinch grasp configurations optimizing its robust grasping performance for specific objects. The hand can be replicated using off the shelf materials and rapid prototyping techniques, while its efficiency has been validated using an extensive set of experimental paradigms.

Ongoing work is focusing on the utilization of the proposed robot hands to the humanoid robot *ESCHER* [34] to increase its ability to manipulate various tools.

Bibliography

- [1] GK Ananthasuresh, Sridhar Kota, and Yogesh Gianchandani. A methodical approach to the synthesis of micro compliant mechanisms. In *Technical Digest, Solid-States Sensor and Actuator Workshop*, pages 189–192, 1994.
- [2] Konstantinos Andrianesis and Anthony Tzes. Development and control of a multifunctional prosthetic hand with shape memory alloy actuators. *Journal of Intelligent & Robotic Systems*, 78(2):257–289, 2015.
- [3] Daniel M Aukes, Barrett Heyneman, John Ulmen, Hannah Stuart, Mark R Cutkosky, Susan Kim, Pablo Garcia, and Aaron Edsinger. Design and testing of a selectively compliant underactuated hand. *The International Journal of Robotics Research*, 33(5):721–735, 2014.
- [4] Ravi Balasubramanian, Joseph T Belter, and Aaron M Dollar. Disturbance response of two-link underactuated serial-link chains. *Journal of Mechanisms and Robotics*, 4(2):021013, 2012.
- [5] Martin Philip Bendsøe and Noboru Kikuchi. Generating optimal topologies in structural design using a homogenization method. *Computer Methods in Applied Mechanics and Engineering*, 71(2):197–224, 1988.
- [6] Antonio Bicchi. Hands for dexterous manipulation and robust grasping: A difficult road toward simplicity. *IEEE Transactions on Robotics and Automation*, 16(6):652–662, 2000.

- [7] Lionel Birglen and Clément M Gosselin. Kinetostatic analysis of underactuated fingers. *IEEE Transactions on Robotics and Automation*, 20(2):211–221, 2004.
- [8] Lionel Birglen, Thierry Laliberté, and Clément M Gosselin. *Underactuated robotic hands*. Springer, 2007.
- [9] Christopher Y Brown and H Harry Asada. Inter-finger coordination and postural synergies in robot hands via mechanical implementation of principal components analysis. In *IEEE/RSJ International Conference on Intelligent Robots and Systems*, pages 2877–2882, 2007.
- [10] Bryan Buchholz, Thomas J Armstrong, and Steven A Goldstein. Anthropometric data for describing the kinematics of the human hand. *Ergonomics*, 35(3):261–273, 1992.
- [11] Vishalini Bundhoo, Edmund Haslam, Benjamin Birch, and Edward J Park. A shape memory alloy-based tendon-driven actuation system for biomimetic artificial fingers, part I: Design and evaluation. *Robotica*, 27(1):131–146, 2009.
- [12] Jörg Butterfaß, Markus Grebenstein, Hong Liu, and Gerd Hirzinger. DLR-Hand II: Next generation of a dextrous robot hand. In *IEEE International Conference on Robotics and Automation*, volume 1, pages 109–114, 2001.
- [13] Manuel G Catalano, Giorgio Grioli, Edoardo Farnioli, Alessandro Serio, Cristina Piazza, and Antonio Bicchi. Adaptive synergies for the design and control of the Pisa/IIT SoftHand. *The International Journal of Robotics Research*, 33(5):768–782, 2014.
- [14] T. Chen, M. Haas-Heger, and M. Ciocarlie. Underactuated hand design using mechanically realizable manifolds. In *IEEE International Conference on Robotics and Automation*, pages 7392–7398, 2018.

- [15] Matei Ciocarlie, Andrew Miller, and Peter Allen. Grasp analysis using deformable fingers. In *IEEE/RSJ International Conference on Intelligent Robots and Systems*, pages 4122–4128, 2005.
- [16] Matei Ciocarlie, Fernando Mier Hicks, Robert Holmberg, Jeffrey Hawke, Michael Schlicht, Jeff Gee, Scott Stanford, and Ryan Bahadur. The Velo gripper: A versatile single-actuator design for enveloping, parallel and fingertip grasps. *The International Journal of Robotics Research*, 33(5):753–767, 2014.
- [17] Matei T Ciocarlie and Peter K Allen. Hand posture subspaces for dexterous robotic grasping. *The International Journal of Robotics Research*, 28(7):851–867, 2009.
- [18] P Coulet, J-M Gilli, and G Rousseaux. On the critical equilibrium of the spiral spring pendulum. In *Proceedings of the Royal Society of London A: Mathematical, Physical and Engineering Sciences*, pages 407–421, 2009.
- [19] Mark R Cutkosky and Sangbae Kim. Design and fabrication of multi-material structures for bioinspired robots. *Philosophical Transactions of the Royal Society of London A: Mathematical, Physical and Engineering Sciences*, 367(1894):1799–1813, 2009.
- [20] Nikhil Chavan Daffe, Alberto Rodriguez, Robert Paolini, Bowei Tang, Siddhartha S Srinivasa, Michael Erdmann, Matthew T Mason, Ivan Lundberg, Harald Staab, and Thomas Fuhlbrigge. Extrinsic dexterity: In-hand manipulation with external forces. In *IEEE International Conference on Robotics and Automation*, pages 1578–1585, 2014.
- [21] Skyler A Dalley, Tuomas E Wiste, Thomas J Withrow, and Michael Goldfarb. Design of a multifunctional anthropomorphic prosthetic hand with extrinsic actuation. *IEEE/ASME Transactions on Mechatronics*, 14(6):699–706, 2009.
- [22] Raphael Deimel and Oliver Brock. A novel type of compliant and underactuated robotic

- hand for dexterous grasping. *The International Journal of Robotics Research*, 35(1-3): 161–185, 2016.
- [23] Cosimo Della Santina, Giorgio Grioli, Manuel Catalano, Alberto Brando, and Antonio Bicchi. Dexterity augmentation on a synergistic hand: The Pisa/IIT SoftHand+. In *IEEE/RAS International Conference on Humanoids Robots*, pages 497–503, 2015.
- [24] Cosimo Della Santina, Cristina Piazza, Giorgio Grioli, Manuel G Catalano, and Antonio Bicchi. Toward dexterous manipulation with augmented adaptive synergies: The Pisa/IIT SoftHand 2. *IEEE Transactions on Robotics*, (99):1–16, 2018.
- [25] Louis-Alexis Allen Demers and Clément Gosselin. Kinematic design of a planar and spherical mechanism for the abduction of the fingers of an anthropomorphic robotic hand. In *IEEE International Conference on Robotics and Automation*, pages 5350–5356, 2011.
- [26] Ashish D Deshpande, Zhe Xu, Michael J Vande Weghe, Benjamin H Brown, Jonathan Ko, Lillian Y Chang, David D Wilkinson, Sean M Bidic, and Yoky Matsuoka. Mechanisms of the anatomically correct testbed hand. *IEEE/ASME Transactions on Mechatronics*, 18(1):238–250, 2013.
- [27] Aaron M Dollar and Robert D Howe. The highly adaptive SDM hand: Design and performance evaluation. *The International Journal of Robotics Research*, 29(5):585–597, 2010.
- [28] Julio Fajardo, Victor Ferman, Ali Lemus, and Eric Rohmer. An affordable open-source multifunctional upper-limb prosthesis with intrinsic actuation. In *IEEE Workshop on Advanced Robotics and its Social Impacts*, pages 1–6, 2017.

- [29] Larry L Howell. Compliant mechanisms. In *Encyclopedia of Nanotechnology*, pages 457–463. Springer, 2012.
- [30] Larry L Howell and A Midha. A method for the design of compliant mechanisms with small-length flexural pivots. *Journal of Mechanical Design*, 116(1):280–290, 1994.
- [31] IA Kapandji. *Physiology of the joints: Upper limb*, volume 1. Churchill Livingstone Edinburgh, 6 edition, 1974.
- [32] Haruhisa Kawasaki, Tsuneo Komatsu, and Kazunao Uchiyama. Dexterous anthropomorphic robot hand with distributed tactile sensor: Gifu hand II. *IEEE/ASME Transactions on Mechatronics*, 7(3):296–303, 2002.
- [33] Sangbae Kim, Alan T Asbeck, Mark R Cutkosky, and William R Provancher. SpinybotII: Climbing hard walls with compliant microspines. In *International Conference on Advanced Robotics*, pages 601–606, 2005.
- [34] Coleman Knabe, Robert Griffin, James Burton, Graham Cantor-Cooke, Lakshitha Dantanarayana, Graham Day, Oliver Ebeling-Koning, Eric Hahn, Michael Hopkins, Jordan Neal, et al. Team VALOR’s ESCHER: A novel electromechanical biped for the darpa robotics challenge. *Journal of Field Robotics*, 34(5):912–939, 2017.
- [35] George P Kontoudis. Design and development of an underactuated, anthropomorphic robot hand. Diploma thesis, National Technical University of Athens, 2016.
- [36] George P Kontoudis, Minas Liarokapis, Agisilaos G Zisimatos, Christoforos I Mavrogiannis, and Kostas J Kyriakopoulos. Open-source, anthropomorphic, underactuated robot hands with a selectively lockable differential mechanism: Towards affordable prostheses. In *IEEE/RSJ International Conference on Intelligent Robots and Systems*, pages 5857–5862, 2015.

- [37] Sridhar Kota, Jinyong Joo, Zhe Li, Steven M Rodgers, and Jeff Sniegowski. Design of compliant mechanisms: Applications to MEMS. *Analog Integrated Circuits and Signal Processing*, 29(1-2):7–15, 2001.
- [38] Pei-Hsin Kuo and Ashish D Deshpande. A novel joint design for robotic hands with humanlike nonlinear compliance. *Journal of Mechanisms and Robotics*, 8(2):021004 1–10, 2016.
- [39] Frank L Lewis, Draguna L Vrabie, and Vassilis L Syrmos. *Optimal control*. John Wiley & Sons., 3 edition, 2012.
- [40] Minas Liarokapis, Panagiotis K Artemiadis, and Kostas J Kyriakopoulos. Quantifying anthropomorphism of robot hands. In *IEEE International Conference on Robotics and Automation*, pages 2041–2046, 2013.
- [41] Minas Liarokapis, Agisilaos G Zisimatos, Christoforos I Mavrogiannis, and Kostas J Kyriakopoulos. OpenBionics: An open-source initiative for the creation of affordable, modular, light-weight, underactuated robot hands and prosthetic devices. In *2nd ASU Rehabilitation Robotics Workshop*, 2014.
- [42] Minas V Liarokapis, Agisilaos G Zisimatos, Melina N Bousiou, and Kostas J Kyriakopoulos. Open-source, low-cost, compliant, modular, underactuated fingers: Towards affordable prostheses for partial hand amputations. In *IEEE International Conference of the Engineering in Medicine and Biology Society*, pages 2541–2544, 2014.
- [43] Nicolae Lobontiu, Jeffrey SN Paine, Ephraim Garcia, and Michael Goldfarb. Corner-filletted flexure hinges. *Journal of Mechanical Design*, 123(3):346–352, 2001.
- [44] Fabrizio Lotti, Paolo Tiezzi, Gabriele Vassura, Luigi Biagiotti, Gianluca Palli, and

- Claudio Melchiorri. Development of UB hand 3: Early results. In *IEEE International Conference on Robotics and Automation*, pages 4488–4493, 2005.
- [45] CS Lovchik and Myron A Diftler. The robonaut hand: A dexterous robot hand for space. In *IEEE International Conference on Robotics and Automation*, volume 2, pages 907–912, 1999.
- [46] Raymond R Ma and Aaron M Dollar. Linkage-based analysis and optimization of an underactuated planar manipulator for in-hand manipulation. *Journal of Mechanisms and Robotics*, 6(1):011002, 2014.
- [47] Raymond R Ma, Joseph T Belter, and Aaron M Dollar. Hybrid deposition manufacturing: Design strategies for multimaterial mechanisms via three-dimensional printing and material deposition. *Journal of Mechanisms and Robotics*, 7(2):021002, 2015.
- [48] Raymond R Ma, Adam Spiers, and Aaron M Dollar. M² gripper: Extending the dexterity of a simple, underactuated gripper. In *IEEE/IFToMM International Conference on Reconfigurable Mechanisms and Robotics*, pages 795–805, 2016.
- [49] Rahim Mutlu, Gursel Alici, Marc in het Panhuis, and Geoffrey M Spinks. 3D printed flexure hinges for soft monolithic prosthetic fingers. *Soft Robotics*, 3(3):120–133, 2016.
- [50] Taylor D Niehues, Raymond J King, Ashish D Deshpande, and Sean Keller. Development and validation of modeling framework for interconnected tendon networks in robotic and human fingers. In *IEEE International Conference on Robotics and Automation*, pages 4181–4186, 2017.
- [51] Lael U Odhner and Aaron M Dollar. The smooth curvature model: An efficient representation of Euler–Bernoulli flexures as robot joints. *IEEE Transactions on Robotics*, 28(4):761–772, 2012.

- [52] Lael U Odhner, Leif P Jentoft, Mark R Claffee, Nicholas Corson, Yaroslav Tenzer, Raymond R Ma, Martin Buehler, Robert Kohout, Robert D Howe, and Aaron M Dollar. A compliant, underactuated hand for robust manipulation. *The International Journal of Robotics Research*, 33(5):736–752, 2014.
- [53] Tariq Rahman, Rungun Ramanathan, Rahamim Seliktar, and William Harwin. A simple technique to passively gravity-balance articulated mechanisms. *Journal of Mechanical Design*, 117(4):655–658, 1995.
- [54] Sungmoo Ryew and Hyoukryeol Choi. Double active universal joint (DAUJ): Robotic joint mechanism for human-like motions. *IEEE Transactions on Robotics and Automation*, 17(3):290–300, 2001.
- [55] Joaquín L Sancho-Bru, Marta C Mora, Beatriz E León, Antonio Pérez-González, José L Iserte, and Antonio Morales. Grasp modelling with a biomechanical model of the hand. *Computer Methods in Biomechanics and Biomedical Engineering*, 17(4):297–310, 2014.
- [56] Marco Santello, Martha Flanders, and John F Soechting. Postural hand synergies for tool use. *Journal of Neuroscience*, 18(23):10105–10115, 1998.
- [57] Umberto Scarcia, Giovanni Berselli, Gianluca Palli, and Claudio Melchiorri. Modeling, design, and experimental evaluation of rotational elastic joints for underactuated robotic fingers. In *IEEE-RAS International Conference on Humanoid Robotics*, pages 353–358, 2017.
- [58] Smmoth-On. PMC-780 DRY. [Online]. Available: <https://www.smooth-on.com/products/pmc-780-dry/>, December 2018.
- [59] Hannah Stuart, Shiquan Wang, Oussama Khatib, and Mark R Cutkosky. The ocean one

- hands: An adaptive design for robust marine manipulation. *The International Journal of Robotics Research*, 36(2):150–166, 2017.
- [60] Li Tian, Nadia Magnenat Thalmann, Daniel Thalmann, and Jianmin Zheng. The making of a 3d-printed, cable-driven, single-model, lightweight humanoid robotic hand. *Frontiers in Robotics and AI*, 4:65, 2017.
- [61] Cai-Hua Xiong, Wen-Rui Chen, Bai-Yang Sun, Ming-Jin Liu, Shi-Gang Yue, and Wen-Bin Chen. Design and implementation of an anthropomorphic hand for replicating human grasping functions. *IEEE Transactions on Robotics*, 32(3):652–671, 2016.
- [62] Zhe Xu and Emanuel Todorov. Design of a highly biomimetic anthropomorphic robotic hand towards artificial limb regeneration. In *IEEE International Conference on Robotics and Automation*, pages 3485–3492, 2016.
- [63] Zhe Xu, Vikash Kumar, Yoky Matsuoka, and Emanuel Todorov. Design of an anthropomorphic robotic finger system with biomimetic artificial joints. In *IEEE-RAS/EMBS International Conference on Biomedical Robotics and Biomechatronics*, pages 568–574, 2012.
- [64] Olgierd Cecil Zienkiewicz, Robert Leroy Taylor, and Robert Leroy Taylor. *The finite element method: Solid mechanics*, volume 2. Butterworth-Heinemann, 2000.
- [65] Agisilaos G Zisimatos, Minas Liarokapis, Christoforos I Mavrogiannis, and Kostas J Kyriakopoulos. Open-source, affordable, modular, light-weight, underactuated robot hands. In *IEEE/RSJ International Conference on Intelligent Robots and Systems*, pages 3207–3212, 2014.